ACS MATERIALS Au
AN OPEN ACCESS JOURNAL OF THE AMERICAN CHEMICAL SOCIETY

pubs.acs.org/materialsau

Review

Toward Multicomponent Single-Atom Catalysis for Efficient Electrochemical Energy Conversion

Jaehyun Kim,[‖] Sungkyun Choi,[‖] Jinhyuk Cho,[‖] Soo Young Kim,* and Ho Won Jang*

Cite This: *ACS Mater. Au* 2022, 2, 1−20

Read Online

ACCESS | Metrics & More | Article Recommendations

ABSTRACT: Single-atom catalysts (SACs) have recently emerged as the ultimate solution for overcoming the limitations of traditional catalysts by bridging the gap between homogeneous and heterogeneous catalysts. Atomically dispersed identical active sites enable a maximal atom utilization efficiency, high activity, and selectivity toward the wide range of electrochemical reactions, superior structural robustness, and stability over nanoparticles due to strong atomic covalent bonding with supports. Mononuclear active sites of SACs can be further adjusted by engineering with multicomponent elements, such as introducing dual-metal active sites or additional neighbor atoms, and SACs can be regarded as multicomponent SACs if the surroundings of the active sites or the active sites themselves consist of multiple atomic elements. Multicomponent engineering offers an increased combinational diversity in SACs and unprecedented routes to exceed the theoretical catalytic performance limitations imposed by single-component scaling relationships for adsorption and transition state energies of reactions. The precisely designed structures of multicomponent SACs are expected to be responsible for the synergistic optimization of the overall electrocatalytic performance by beneficially modulating the electronic structure, the nature of orbital filling, the binding energy of reaction intermediates, the reaction pathways, and the local structural transformations. This Review demonstrates these synergistic effects of multicomponent SACs by highlighting representative breakthroughs on electrochemical conversion reactions, which might mitigate the global energy crisis of high dependency on fossil fuels. General synthesis methods and characterization techniques for SACs are also introduced. Then, the perspective on challenges and future directions in the research of SACs is briefly summarized. We believe that careful tailoring of multicomponent active sites is one of the most promising approaches to unleash the full potential of SACs and reach the superior catalytic activity, selectivity, and stability at the same time, which makes SACs promising candidates for electrocatalysts in various energy conversion reactions.

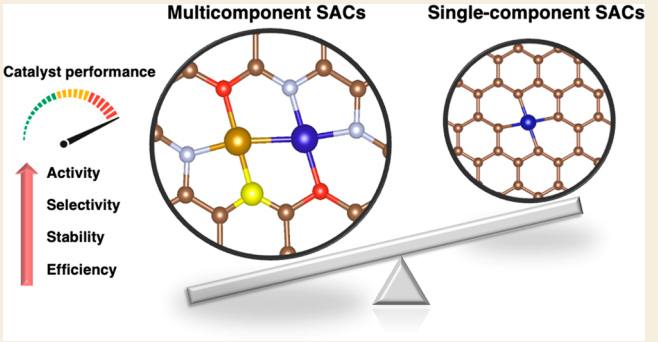

KEYWORDS: *single-atom catalysts, multicomponent, multicomponent single-atom catalysts, dual-metal active site, electrocatalysts, catalyst design, atomic coordination engineering*

INTRODUCTION

Environmental concerns consistently grow as global fossil-fuel consumption and energy demands escalate rapidly, which calls for urgent renewable energy sources and storage developments.[1−5] Currently, electrochemical energy conversions, such as water splitting, fuel cells, and electrochemical reduction of carbon dioxide, are the most critical parts of the sustainable energy production chain.[6−10] The energy from these conversion reactions can be stored in electrochemical energy storage like a metal-air battery.[11] Since catalysts significantly play major roles in accelerating electrochemical reactions, appropriate and advanced electrocatalysts are at the heart of solving the global energy crisis. It has motivated researchers to put extensive efforts into designing and developing new catalysts, including homogeneous and heterogeneous catalysts, in past decades.[12] Homogeneous catalysts offer high catalytic activity and selectivity with identical active sites, adjusted by modifying the active metal centers or their surroundings. Modulated electronic structures of the active sites due to synergistic interactions between catalytic metal sites and support materials also give the opportunity to enhance the heterogeneous catalysts with robustness and technical readiness. Until now, transition metals or noble metals and their oxides have been widely used as catalysts for various electrochemical reactions, and approaches to changing their

Received: August 31, 2021
Revised: October 5, 2021
Accepted: October 5, 2021
Published: October 25, 2021

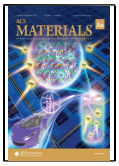

ACS Publications

© 2021 The Authors. Published by American Chemical Society

https://doi.org/10.1021/acsmaterialsau.1c00041
ACS Mater. Au 2022, 2, 1−20

morphology as nanoparticles for advantageous specific surface area and enhanced electronic features have been extensively reported.[13] Unfortunately, the size dispersions of metal or metal oxide nanoparticles inevitably occur, disturbing the catalytic selectivity and efficient atomic utilization.

Single-atom catalysts (SACs) have been regarded as the ultimate solutions that can bridge the gap between those two different classes of catalysts since SACs inherit the advantages of both homogeneous and heterogeneous catalysts.[14−23] Also, the mononuclear nature of SACs enables maximal atom utilization efficiency, high activity, and selectivity toward the wide range of electrochemical reactions, superior structural robustness, and stability over nanoparticles due to strong atomic covalent bonding with supports.[24−33]

Moreover, SACs can be regarded as multicomponent SACs if the surroundings of the active sites or the active sites themselves are engineered with multiple atomic elements, such as introducing dual-metal active sites or additional neighboring atoms (Figure 1), which offers unprecedented routes to

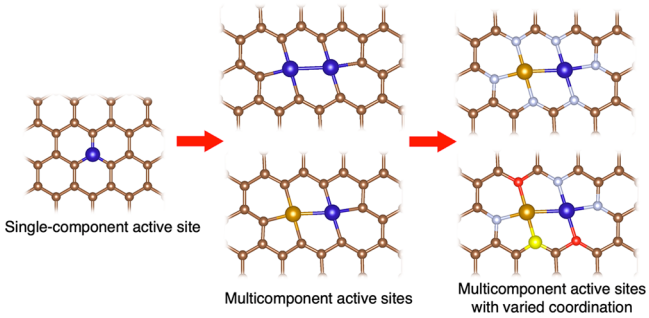

Figure 1. Schematic of SACs with multicomponent active sites embedded in graphene supports.

overcome the lack of combinational diversity in mononuclear SACs and bypass the bottlenecks of scaling relationships for adsorption and transition state energies of reactions that have constrained catalysts performance with theoretical upper-bounds.[34−43] Multicomponent SACs are expected to exceed the bounds imposed by the single-component volcano relationships, thanks to synergistic communications within multicomponent natures, and to realize an optimized catalytic activity, selectivity, and stability. In detail, enhancing atomic active sites of SACs toward multicomponent active sites strongly influences the electronic structure, the nature of orbital filling, the binding energy of reaction intermediates, reaction pathways, and local structural transformations, which leads to substantial differences in the overall electrocatalytic performance. Therefore, careful tailoring of active sites is one of the most promising approaches to unleash the full potential of SACs and reach superior catalytic activity, selectivity, and stability at the same time.

Furthermore, the tunability of SACs can be even more improved by adjusting the coordination environments of the active metal sites in SACs, such as changing the elements or coordination number of the first-neighbor coordination atoms, adding additional ligands, altering the coordination of second- or higher-neighbor shells for synergistic neighboring effects, or replacing with different support materials.[44−46] Fabricating SACs with multicomponent active sites is also critical to experimentally validate the catalytic enhancement, and synthetic strategies, such as defect engineering, metal−support interaction, heteroatom tethering, spatial confinement, atomic alloying, molecular bridging, or metal−organic framework (MOF) derivatization, have emerged to prepare SACs with a tuned environment of the multicomponent active sites.

This Review will introduce how the multicomponent active sites of SACs are responsible for the enhanced catalytic performance by highlighting recent representative publications about multicomponent single-atom catalysis in electrochemical energy conversion reactions. Then, we will demonstrate some general synthesis strategies in preparing SACs and briefly introduce the achievements that have successfully extended these synthesis methods to prepare multicomponent SACs. Characterization techniques for the multicomponent nature of active sites and their coordination environments on an atomic scale will also be illustrated since they are vital for further investigation of SACs with definitive structural information. Finally, current challenges in the research fields of SACs and strategies to overcome these challenges will be summarized. We hope this Review sheds light on the research direction toward multicomponent SACs to rationally maximize and optimize the catalytic performance on a wide range of electrochemical reactions.

ELECTROCHEMICAL APPLICATIONS OF MULTICOMPONENT SACs

Atomically dispersed multicomponent active sites on the support materials enable additional opportunity materials for variable electrochemical energy conversion applications, outperforming most of the state-of-the-art SACs with the single-component active site.[47−53] SACs can be optimized by tailoring the metal atoms, adjacent coordinative dopants, metal loading, and ligand adsorption to fully unleash their potential. The rational design of multicomponent active metal sites and coordination environments has all the advantages of homogeneous catalysis and heterogeneous catalysis, which leads to desired catalysts with superior activity, selectivity, and stability for a wide variety of electrochemical reactions.[45,54−57] We will highlight the recent breakthroughs in SACs, focusing on the impacts of tuning the single-atom sites toward multicomponent active sites with varied coordination on the overall electrocatalytic performance. Experimental and computational advances in understanding the structure−activity relationship between active site modulations of SACs and catalytic performances are summarized and exemplified for the electrochemical applications, including water electrolysis, O_2 reduction, and CO_2 reduction reactions.

Hydrogen Evolution Reaction

Electrochemical water splitting through the hydrogen evolution reaction (HER) provides a sustainable and green route to produce molecular hydrogen for mitigating the global energy crisis. Unfortunately, the development of active catalysts with minimal overpotential and high efficiency is still struggling with the inevitable usage of noble metals, which acts as an obstacle for large-scale industrial applications. Since SACs have intrinsic advantages regarding maximal atomic utilization, every metal atom can theoretically participate in the catalytic reactions as an active site, which eventually increases the mass activity of the metal element and turnover frequency (TOF) of the reactions. The unique structure and electronic properties of SACs have been realized with delicate active site engineering toward multicomponent metal active sites, proven to accelerate the reaction kinetics of HER and scale up the

https://doi.org/10.1021/acsmaterialsau.1c00041
ACS Mater. Au 2022, 2, 1−20

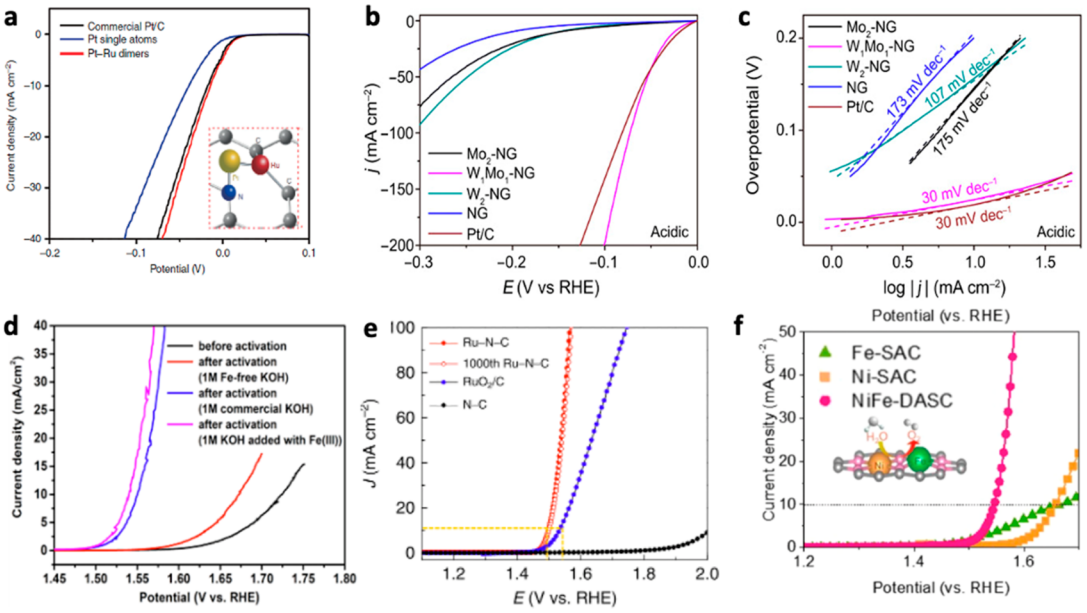

Figure 2. (a) HER polarization curves recorded on Pt−Ru dimers, Pt single atoms, and Pt/C catalysts. Adapted with permission from ref 37. Copyright 2019 Nature Publishing Group. (b, c) Polarization curves and corresponding Tafel plots of Mo_2-NG, W_1Mo_1-NG, W_2-NG, NG, and Pt/C in 0.5 M H_2SO_4. Adapted with permission from ref 36. Copyright 2020 American Association for the Advancement of Science. (d) OER activity evaluated by LSV in 1 M KOH at a scan rate of 5 mV s^{-1} for Co−N−C activated with different 1 M KOH electrolytes with varying Fe ion contents. Reproduced from ref 30. Copyright 2019 American Chemical Society. (e) OER activity evaluated by LSV in 0.5 M H_2SO_4 at a scan rate of 5 mV s^{-1} for Ru−N−C and the commercial RuO_2/C. Adapted with permission from ref 65. Copyright 2019 Nature Publishing Group. (f) OER activity evaluated by LSV in 1 M KOH at a scan rate of 1 mV s^{-1} for Fe-SAC, Ni-SAC, and NiFe-DSAC. Adapted with permission from ref 38. Copyright 2021 Nature Publishing Group.

hydrogen production. SACs based on atomically dispersed noble metal elements, such as Pt, Ir, Ru, Pd, and Rh, have been prepared and examined for various electrochemical applications, including HER electrocatalysis. Also, tremendous efforts from researchers have aimed to replace noble metal with earth-abundant transition metal elements, such as Fe, Co, Ni, and Cu, that hold great promise for clean energy conversion reaction with large-scale application.

For example, Zhou et al. developed a single-atom Pt immobilized NiO/Ni heterostructure supported on Ag nanowires that enable efficient HER in an alkaline electrolyte with a high mass activity of 20.6 A mg^{-1} for Pt at an overpotential of 100 mV.[58] The binding energies of hydroxyl ions and hydrogen into a Pt single atom coupled with NiO/Ni heterostructure were optimized to dissociate H_2O molecules efficiently. Lu et al. also prepared atomically dispersed Ru in N-doped carbon nanowires as effective electrocatalysts for HER. The catalytic activity was higher than that of the commercial Pt/C catalysts, with an overpotential of only −12 mV to reach the current density of 10 mV cm^{-2} in an alkaline electrolyte of 1 M KOH.[59] Density functional theory (DFT) calculation revealed that a Ru atom coordinated with two nitrogen and two carbon atoms, namely, Ru−C_2−N_2, was the most active catalytic center due to lower hydrogen binding energy than that of Ru nanoparticles and lower kinetic barrier for water dissociation than that of Pt catalysts. Both Ru and adjacent carbon atoms were regarded as the possible active sites, which offered unprecedented catalytic mechanisms and performance. Fei et al. developed Co atoms incorporated in N-doped graphene (Co-NG) or undoped graphene (Co-G) via a pyrolysis process.[60] Very small amounts of Co addition altered the N-doped graphene with negligible intrinsic HER activity to a highly active and robust HER catalyst in both acidic and alkaline electrolytes.

Zhang et al. synthesized atomically isolated Pt−Ru bimetallic dimers on nitrogen-doped carbon nanotubes by the deposition of an atomic layer and obtained excellent mass activity and stability compared to commercial Pt/C catalyst for HER (Figure 2a).[37] The mass activity of the Pt−Ru dimer structure of HER at the overpotential of 50 mV was 23.1 A mg^{-1}, which is 54-fold greater than that of the commercial Pt/C catalysts and exceeded that of most other state-of-the-art Pt-based catalysts. Furthermore, additional DFT calculations revealed that the Pt−Ru dimer structure could be easily changed from metal to semiconductor, leaving unoccupied orbitals, and the interaction between Ru atom and H atom could be tuned by the Pt atom adjacent to the Ru atom. Specifically, tuning the number of adsorbed H atoms on either Pt and Ru atoms to more than two or three, Pt−Ru dimer structure lost its metallic behavior and the H atom became easy to detach from Ru atom when the Pt−Ru dimer had the maximum hydrogen coverage. These precise coordination environment modulations resulted in the synergetic effects of HER, accompanied by the optimized adsorption energy of intermediates.

Wang et al. designed atomically dispersed Co and Pt atoms anchored on TiO_2 surfaces to further improve Pt catalytic efficiency in HER.[28] The mass activity of this new catalyst far exceeded the mass activity of equal amounts of Pt single-atom and typical Pt clustered catalysts. Further inspections revealed that neighbor Pt atoms activated Co atoms and the activity of Pt atoms was further enhanced through dimer interaction with Co atoms in the oxygen-coordinated Co−O−Pt structure, which eventually weakened the H adsorbate binding energy

https://doi.org/10.1021/acsmaterialsau.1c00041
ACS Mater. Au 2022, 2, 1−20

and optimized the electronic states of both Pt and Co metal atoms active sites.

Recently, Yang et al. developed a dual-atom catalyst consisting of an O-coordinated W−Mo heterodimer embedded in N-doped graphene (W_1Mo_1-NG),[36] synthesized by controllable self-assembly and nitridation processes. The O-bridged W−Mo atoms in W_1Mo_1-NG were anchored in the vacancies of N-doped graphene through oxygen atoms with a W−O−Mo−O−C configuration, resulting in robust structural stability and well-dispersed atomic moiety distribution. Although W_1Mo_1-NG did not consist of noble metal elements, it clearly exhibited comparable HER catalytic activity to the noble-metal-based commercial Pt/C catalysts and even showed ultrahigh stability for HER in both acidic and alkaline electrolytes. Specifically, W_1Mo_1-NG showed excellent catalytic activity toward HER in acidic electrolytes, giving a near-zero onset potential (U_{onset}), a low cathodic geometric current density (j) of 10 mA cm^{-2} at a very low overpotential of 24 mV (η_{10} = 24 mV), and a small Tafel slope of 30 mV dec^{-1} (Figure 2b, c). W and Mo atoms were located in a oxygen-bridged WO_4 tetrahedron and distorted MoO_6 octahedron, respectively, and the connected W−O−Mo−O−C configuration was proven to delocalize electrons and provide an optimal adsorption strength of H atoms. These local coordination environment engineering with multicomponent atoms accelerated overall HER kinetics with promoted intrinsic activity, thus emphasizing the synergistic impacts of microenvironment modulation on SACs.

Also, Cao et al. prepared P-doped C_3N_4 with immobilized single-Co atom catalysts (Co_1/PCN SACs) and confirmed the geometrically dispersed uniform Co_1-N_4 moiety was responsible for the enhanced HER catalytic activity.[61] Operando X-ray absorption fine structure analysis (XAFS) measurements revealed that the formation of a high-valence $HO-Co_1-N_2$ moiety from the coordination-unsaturated single Co sites easily accelerated the H adsorbate adsorption, due to the preferred dynamic H_2O adsorption as $H_2O-(HO-Co_1-N_2)$.

In a recent work done by Yang et al., a TiC support with a low load-level of anchored Rh single atoms (Rh_1−TiC) was suggested as a promising catalyst candidate toward HER with the combination of the metallic center and the support materials via DFT calculation of electronic metal−support interaction (EMSI).[62] They revealed that a beneficial EMSI with facile electron transfer from the 3d orbitals of the surrounding Ti atoms to the 3d orbitals of the anchored Rh atom might be responsible for the enhanced catalytic activity of metallic Rh active sites in Rh_1−TiC. Superior catalytic performance of Rh_1−TiC was experimentally confirmed with low overpotentials of 22 and 86 mV at the current densities of 10 and 100 mA cm^{-2}, robust stability at 500 mA cm^{-2} for 24 h, and 20% electricity consumption decrease at a practical working condition of 200 mA cm^{-2} compared with the state-of-art Pt/C catalyst.

Nonmetal single atoms can also be the active single-atomic sites of multicomponent SACs. For example, Zhao et al. prepared a single-atom nickel iodide (SANi-I) electrocatalyst with a simple calcination process and reported a superior HER activity achieving an ultralow overpotential of 60 mV at 100 mA cm^{-2}.[63] The atomically dispersed nonmetal iodine atoms easily formed chemical bonds with the hydrogen adatoms and formed $I-H_{ads}$ intermediates, while OH^- from the water dissociation process could be adsorbed on the adjacent Ni atoms, which collaboratively promotes the overall HER process.

Oxygen Evolution Reaction

The water-splitting reaction provides renewable energy resources by transforming electricity into the chemical form of hydrogen fuel. The oxygen evolution reaction (OER) is an essential half-reaction for water splitting and metal−air batteries, which often suffers from sluggish kinetics and large overpotential due to multiproton-coupled electron transfer steps in OER processes. Proton exchange membranes and acidic electrolytes are known for various advantages, such as the high mobility of electronic carriers compared to hydroxyl ions in alkaline water. However, despite the huge advantages of OER in acidic electrolytes, only a few noble metal catalysts could survive at harsh acidic conditions and most of the earth-abundant transition metal catalysts are not stable in acidic electrolytes and high anodic potential ranges of OER, which might lead to severe corrosion.

For example, Fei et al. investigated the MN_4C_4 (M = Fe, Co, and Ni) moieties embedded in a graphene matrix and suggested a dual-site mechanism for NiN_4C_4 SACs where the *OOH adsorbates in the OER process prefer to bond with the Ni site but the *O and *OH adsorbates prefer to bond with the carbon atom adjacent to the Ni metal atom, and the definitive structure identification provided a key clue to understand catalytic activity.[64] Without considering the dual-site mechanisms, DFT calculations on NiN_4C_4 that regarded only Ni metal as an active center predicted that NiN_4C_4 had the highest limiting potential in the OER process compared to the SACs with M = Co or Fe, which did not match up with the experimental result. The unambiguous structure determination via systematic X-ray absorption fine structure analysis (XAFS) and direct transmission electron microscopy (TEM) imaging confirmed the geometrical structures that were further studied with DFT calculation. Furthermore, the trend of OER activities of M−N−C was predicted as following Ni > Co > Fe, which agreed with the electrochemical measurement results.

Bai et al. reported that Co−Fe dual-atom catalysts embedded in N-doped carbon could be prepared by the electrochemical activation of single-atom Co species atomically dispersed on N-doped carbon in Fe-containing alkaline electrolyte.[30] This novel Fe-incorporation strategy in situ transformed single-atom Co into Co−Fe dimer structures that act as the active site of the catalysts, confirmed with operando X-ray absorption spectroscopy. Specifically, the $Fe(NO_3)_3 \cdot 9H_2O$ precursor was added into the KOH electrolyte, and OER catalytic performance was enhanced as the overpotential at 10 mA cm^{-2} was decreased to 309 mV (Figure 2d). These results supported that Fe incorporation caused a structural change of the single-atom Co site during the activation step, which was essential for the high activity of Co−N−C. The presence of a new Co species formed upon Fe incorporation upon positive potentials, where the $[Fe(OH)_4]^-$ species tend to be absorbed onto the electrode. Since the atomically dispersed Co sites are the preferred sites for $[Fe(OH)_4]^-$ absorption, the activated Co−N−C catalyst gave rise to the modulated coordination environments with multicomponent dimeric Co−Fe. This Co−Fe dual-atom catalyst exhibited the highest turnover frequencies among metal oxides and excellent stability during the OER.

Cao et al. developed active and stable OER electrocatalysts in an acid electrolyte that unlock the potential of proton

https://doi.org/10.1021/acsmaterialsau.1c00041
ACS Mater. Au 2022, 2, 1−20

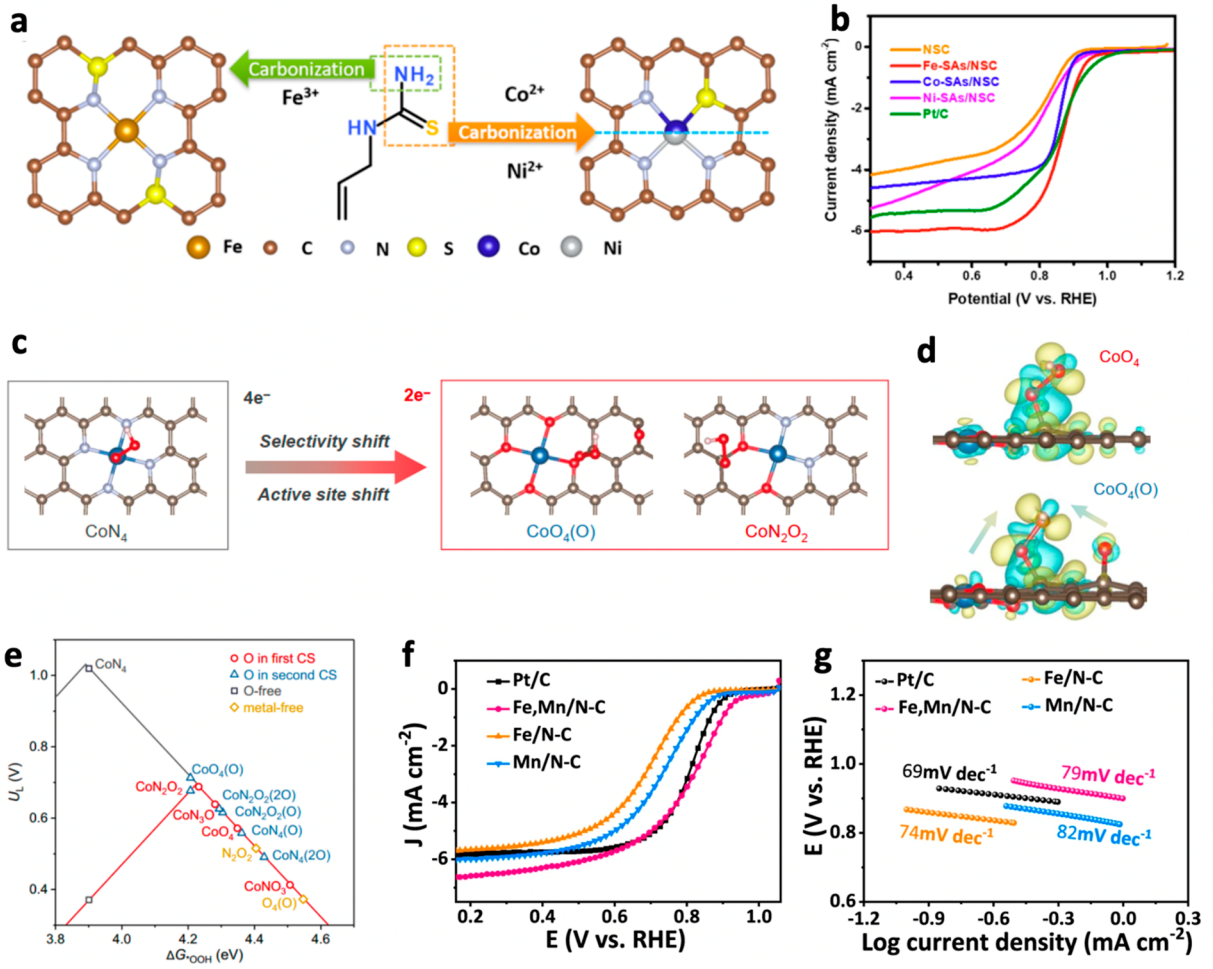

Figure 3. (a) Schematic illustration of the formation of Fe-SAs/NSC, Co-SAs/NSC, and Ni-SAs/NSC with different coordination environments. (b) ORR polarization curves of NSC, Ni-SAs/NSC, Co-SAs/NSC, Fe-SAs/NSC, and Pt/C in O_2-saturated 0.1 M KOH solution with a rotation rate of 1600 rpm. (a, b) Reproduced from ref 68. Copyright 2019 American Chemical Society. (c) Optimized geometry structures of *OOH adsorption on CoN_4, $CoO_4(O)$, and CoN_2O_2 moieties illustrated with a preferred ORR pathway. (d) Differential charge densities of CoO_4 and $CoO_4(O)$ after *OOH adsorption. Yellow- and cyan-colored isosurfaces show electron gain and loss, respectively. (e) Computed activity volcano plots of ORR via the two-electron (red color) or four-electron (black color) pathway for SACs with varied configurations. (c–e) Reproduced from ref 71. Copyright 2021 American Chemical Society. (f) LSV curves of (Fe, Mn)/N–C, Fe/N–C, Mn/N–C, and Pt/C catalysts in O_2-saturated 0.1 M $HClO_4$ solution. (g) Corresponding Tafel plots obtained from the RDE polarization curves. (f, g) Adapted with permission from ref 35. Copyright 2021 Nature Publishing Group.

exchange membrane assisted water electrolysis for a cost-effective and sustainable energy supply with an atomically dispersed Ru atom coordinated with four N dopants and embedded in a carbon support.[65] The Ru–N–C electrocatalysts delivered a remarkably high intrinsic activity and TOF and showed no evident dissolution after 30 h of operation in acidic environments. Superior stability was enabled by oxygen-free environments that suppress the lattice oxygen evolution reaction and strong Ru–N bonds that prevent Ru atoms from dissolving. Also, the preadsorbed O atom in the Ru atom site resulted in multicomponent modulated coordination of the $O–Ru_1–N_4$ moiety that induced the Ru atom to donate more electrons to the electronegative O atom and the average Ru oxidation states increased, which was responsible for the high OER activity and stability. A low overpotential of 267 mV at a current density of 10 mA cm^{-2} confirmed Ru–N–C as being more efficient in OER than commercial RuO_2/C in 0.5 M H_2SO_4 electrolyte (Figure 2e).

Han et al. developed atomically dispersed Co–Ni dimer sites embedded in N-doped hollow carbon nanocubes via pyrolysis of dopamine-coated metal–organic frameworks.[25] Outstanding catalytic performances in both OER and oxygen reduction reaction (ORR) were confirmed, and this bifunctionality could be applied in manufacturing realistic rechargeable Zn-air batteries with superior efficiency, decreased overpotential, and consistent reversibility. Additional DFT calculations demonstrated that the synergistic effect of neighboring Co–Ni dual metal center and atomically dispersed single atoms resulted from the optimized binding energy of intermediates in multicomponent modulated active metal sites, which decreased overall reaction barriers.

Recently, Zeng et al. successfully synthesized a diatomic Ni–Fe catalyst anchored in N-doped graphene, and it exhibited decent electrocatalytic activities and stability for OER via orbital coupling between the catalytic Fe center and the adjacent Ni atom.[38] The oxidation state of Fe became higher, and binding strength to the reaction intermediates was

https://doi.org/10.1021/acsmaterialsau.1c00041
ACS Mater. Au 2022, 2, 1–20

weakened, which showed higher OER catalytic performance with lower overpotential than Fe or Ni single atoms embedded in N-doped carbon for OER in 1 M KOH electrolyte (Figure 2f). This multicomponent SAC also showed outstanding electrocatalytic activities and stability for CO_2RR at the voltage potential range different from the oxidative potentials for OER. The bifunctionality for OER and CO_2RR is desirable for the electrode materials of the rechargeable Zn-CO_2 battery, and the researchers built the rechargeable Zn-CO_2 battery cell to test the discharge−charge cycles and tried to bridge the gap between research result in laboratory condition and the practical implementation.

Support materials for the single atoms in SACs are not limited to carbon-based materials. For example, Shan et al. integrated Ir single atoms into the cationic sites of the cobalt spinel oxide lattice.[66] They revealed that the identical local atomic structural environment of correlated Ir single atoms in the host cobalt oxide lattice was responsible for the enhanced catalytic OER activity by beneficially modifying the electronic structure. Among the atomically correlated $Ir_xCo_{1-x}O_4$ with different compositions of the integrated Ir component x, $Ir_{0.06}Co_{2.94}O_4$ showed the best OER mass activity and also outperformed the conventional surface adsorbed Ir single atoms on a Co_3O_4 support (Ir SA@Co_3O_4). The atomic correlations of Ir with Co and O in the host lattice also improved corrosion resistance in acidic $HClO_4$ electrolyte solution and under oxidative electronic potentials. In addition, Li et al. reported stabilized Pt single atoms on PtCo alloy nanosheets with trapped interstitial fluorine (SA-PtCoF) by electrodeposition and fluorine plasma treatment.[67] The Pt−Co bond in PtCo alloy nanosheets was weakened by the lattice distortion induced by the interstitial F atoms, which eventually stabilized atomically dispersed Pt in the SA-PtCoF and further enhanced OER activity with low onset potential of 1.50 V. Since, the SA-PtCoF also showed the onset potential of 0.95 V for ORR superior to the commercial Pt@RuO_2, SA-PtCoF was a bifunctional catalyst that exhibited high activity toward both OER and ORR. The bifunctionality of the SA-PtCoF catalyst made it attractive as a cathode in zinc-air batteries (ZABs), and the prepared ZABs with the SA-PtCoF cathode showed superior durability under continuous cycles for over 240 h with a peak power density of 125 mW cm^{-2} and a specific capacity of 808 mA h g_{Zn}^{-1} at 10 mA cm^{-2}. Practical implementation as flexible ZABs for wearable electronics was also reported to ensure the persistent enhancement of multicomponent SACs for practical device-level performance.

Oxygen Reduction Reaction

Platinum is the state-of-the-art catalyst for ORR, but its high cost and scarcity limit its large-scale use. However, if the usage of Pt reduces to a sufficiently low level, this critical barrier may be overcome. Atomically dispersed metal catalysts with high activity and high atom efficiency have the possibility to achieve this goal. Besides only one metal site in the dual-atom catalyst as the active site, both metal sites might engage in the reaction via a different reaction mechanism. For example, the dissociative pathway might be applicable to dual-atom catalysts because of the existence of multiple active sites, which are distinct from SACs. Moreover, ORR can occur via a dual-site reaction mechanism. One metal site is responsible for the reduction of O_2 to H_2O_2, and H_2O_2 can be further reduced to H_2O on the other metal site. Importantly, if both metal sites take part in the reaction, the scaling relationship that limits ORR activity could be broken and a better catalyst could be achieved. The electronic structure and reaction mechanisms of SACs, and hence their catalytic activity, can be tuned by coordinating the center metal atom with other elements, such as S, P, O, N, and B, or constructing dual metal atom catalytic centers.

For example, Zhang et al. synthesized a series of single metal atoms anchored on a porous N, S-codoped carbon (NSC) matrix, namely, FeN_4S_2, CoN_3S_1, and NiN_3S_1, and explored the relationship between structure and ORR catalytic activity.[68] Since no metal−metal bonds were observed in K-edge X-ray absorption near edge structure (XANES) spectra, a single metal atom site coordinated with N, S, or C, definitely not other metal atoms. Unlike Co−S bonds and Ni−S bonds that were observed in the Fourier transformed extended X-ray absorption structure (EXAFS) spectra, Fe−S bonds were not detected; this means that, in the FeN_4S_2 structure, S atoms bond with N atoms adjacent to the center Fe atom and multicomponent coordination environments with four N atoms as first-neighbors and S and C atoms as second-neighbors are present (Figure 3a). DFT calculations revealed that the Fe-centered single atom anchored on porous N, S-codoped carbon was the most active site, superior to the Co or Ni-centered counterparts and even the commercial Pt/C catalysts (Figure 3b), due to the higher charge density and lower energy barrier of the intermediates during ORR.

The multielectron process of the acidic ORR can occur via a two-electron pathway to produce H_2O_2 or via a four-electron pathway to produce H_2O, and multicomponent SACs with atomic-level tuned surroundings of the active sites can selectively favor one specific ORR pathway over the other ORR pathway. For the case of Co-SACs as an example, Wu et al. reported a single-atom Co−N_4 electrocatalyst embedded in porous carbon nanospheres that selectively pursue ORR in neutral media with the four-electron pathway, not the two-electron pathway resulting in H_2O_2 production.[69] Since the ratio of the catalytic reduction currents of H_2O_2 and O_2 was determined to be 14% for Co−N_4/C, which was significantly smaller than that of 55% for Pt/C or 57% for Pt electroplated on glassy carbon electrode (Pt-GCE), Co−N_4/C showed a high tolerance to the H_2O_2 producing two-electron pathway. Electrochemical kinetic analysis revealed that the direct four-electron pathway was exclusively chosen rather than the two sequential two-electron reduction pathways with a dissociable H_2O_2 intermediate, and further DFT calculations also indicated that the weak adsorption of H_2O_2 on the porphyrin-like Co−N_4 site might cause the selectivity toward the four-electron pathway. On the other hand, Jung et al. tuned a surrounding atomic configuration of a Co−N_4 moiety incorporated in nitrogen-doped graphene with additional adsorbed oxygen atoms, denoted as CoN_4(O), and a high H_2O_2 selectivity of 82% was confirmed with a predominance of the two-electron pathway over the four-electron pathway.[70] This contradiction in Co-SACs was resolved by Tang et al. revealing a role of the surrounding atomic coordination in ORR pathway selection (Figure 3c).[71] Charge difference analysis demonstrated that the adsorbed oxygen atoms adjacent to Co−N_4 or Co−O_4 moieties induce a directional electron depletion of Co toward the *OOH adsorption site, which was advantageous to the two-electron pathway (Figure 3d). Varying the configuration of the first and second coordination spheres in SACs, computed activity volcano plots of ORR were constructed with the binding free energy of

https://doi.org/10.1021/acsmaterialsau.1c00041
ACS Mater. Au 2022, 2, 1−20

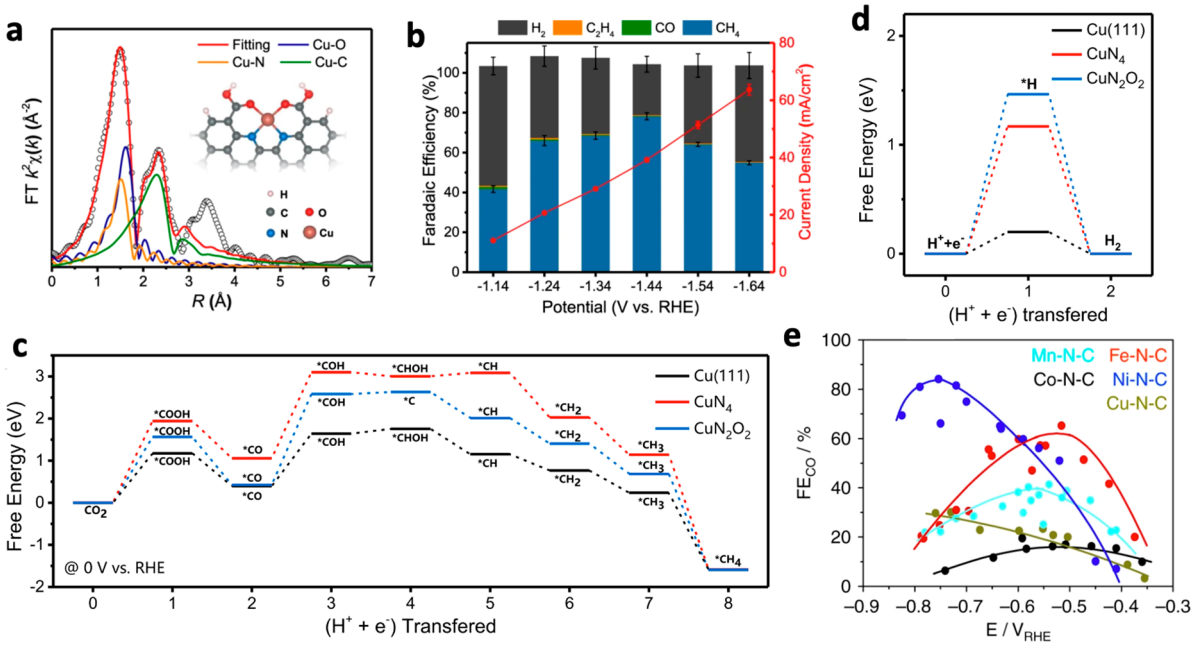

Figure 4. (a) EXAFS fitting curves of Cu-CDs in *R* space using backscattering paths of Cu−N, Cu−O, and Cu−C. The inset in (a) shows the structure of Cu sites in Cu-CDs. (b) Dependence of faradaic efficiency and current density based on geometric surface area of Cu-CDs with Cu−N/O-C structures. (c) Free energy diagram of CO_2 reduction pathway to CH_4 and (d) HER pathway on the CuN_2O_2(Cu-CDs), CuN_4, and Cu(111). (a−d) Adapted with permission from ref 76. Copyright 2021 Nature Publishing Group. (e) FE_{CO} versus applied, IR-corrected electrode potential of CO for the five M−N−C catalysts. Adapted with permission from ref 77. Copyright 2017 Nature Publishing Group.

*OOH from DFT calculations and a thermodynamic limiting potential for both the two-electron and four-electron pathways (Figure 3e). By optimizing the electronic structure and *OOH adsorption behavior, the researchers successfully figured out the structure−property relationships of multicomponent SACs in acidic ORR and confirmed that CoO_4 moieties with adjacent additional oxygen atoms incorporated in a carbon matrix exhibit superior catalytic activity and high selectivity of 95% toward acidic H_2O_2 production via the two-electron pathway. In contrast, suppressing H_2O_2 production and pursuing the four-electron pathway is essential in some practical applications of multicomponent SACs. For example, Wang et al. synthesized a catalyst with atomically dispersed CoN_4 moieties embedded in a 3D porous nitrogen-doped carbon matrix and confirmed its preference for the four-electron pathway, which is desirable to the cathode catalysts materials for proton exchange membrane fuel cells (PEMFCs).[72] A superior half-wave potential of 0.80 V versus reversible hydrogen electrode (RHE) was achieved in a challenging acidic condition of 0.5 M H_2SO_4 electrolyte. Therefore, a rational atomic-level structure design of multicomponent SACs is extremely crucial to engineer the reaction mechanisms and eventually show their potential toward practical implementations.

Not only the atomic coordination of the metal active sites but also the metal active sites themselves can be modulated by introducing multicomponent atomic elements. For example, Yang et al. successfully synthesized dual-metal (Fe, Mn) atomically dispersed on N-doped carbon (Fe, Mn/N−C) catalysts and conducted electrochemical evaluations.[35] Dual-metal atomically dispersed Fe, Mn/N−C and the single-atom Fe/N−C and Mn/N−C catalysts were precisely designed to uncover the spin-state formation of 3d orbitals in transition metal ions, which could be useful in optimizing the ORR activity. DFT calculations demonstrated that an average oxidation state of Fe atoms was affected by adjacent atomically dispersed Mn−N moieties, which can effectively activate the Fe(III) sites and permit Fe(III) in FeN_4 to achieve the ideal one e_g electron filling, allowing the excellent ORR activity and selectivity of Fe, Mn/N−C in both alkaline and acidic media (Figure 3f, g). DFT calculations further confirmed that the electronic structure-adjusted Fe, Mn/N−C and the oxygen intermediate had proper bond length and binding energy, which improved the reaction kinetics of ORR. Moreover, Han et al. also recently revealed that the O_2 activity and ORR catalytic activity of the Fe−N_4 moiety could also be enhanced by introducing an adjacent Pt−N_4 moiety without the direct chemical bonding between different metal atoms.[73] The neighboring Fe−N_4 and Pt−N_4 embedded in a nitrogen-doped carbon framework (Fe−N_4/Pt−N_4@NC) showed a remarkable half-wave potential of 0.93 V versus RHE, which was higher than that of Fe−N4@NC and a commercial Pt/C catalyst. A ZAB using Fe−N_4/Pt−N_4@NC as the electrocatalyst on an air cathode was also built, and a high open-circuit voltage of 1.48 V, a peak power density of 200 mW cm^{-2}, and a large discharge specific capacity of 749.9 mA h g^{-1} at 10 mA cm^{-2} were observed. Interestingly, Co−N_4/Pt−N_4@NC and Mn−N_4/Pt−N_4@NC did not exhibit superior ORR performance enhancement, unlike Fe−N_4/Pt−N_4@NC, and further DFT calculations revealed that the electronic structure modulation of M−N_4 moieties (M = Fe, Co, and Mn) induced from the adjacent Pt−N_4 was advantageous to Fe−N_4 with the optimized adsorption energy of intermediates, but negligible or even negative to Co−N_4 and Mn−N_4 due to the excessively strong binding strength between the adsorbates and the active sites of multicomponent SACs.

Carbon Dioxide Reduction Reaction

The electrochemical CO_2 reduction reaction (CO_2RR) is of great importance to tackling the rising CO_2 concentration in

https://doi.org/10.1021/acsmaterialsau.1c00041
ACS Mater. Au 2022, 2, 1−20

the atmosphere. Direct electrochemical reduction of CO_2 to fuels and chemicals using renewable electricity has attracted significant attention partly due to the fundamental challenges related to reactivity and selectivity and partly due to its importance for industrial CO_2-consuming gas diffusion cathodes, which heavily rely on the development of low-cost and efficient electrocatalysts. A variety of materials can be applied as catalysts for CO_2RR, such as iodide-derived copper (ID-Cu) for ethane production[74] or Bi nanospheres for formate production,[75] and a range of heterogeneous and potentially low-cost multicomponent SACs containing earth-abundant elements have recently emerged as promising candidates for the CO_2RR.

For example, Cai et al. prepared N, O-coordinated Cu single atom embedded in carbon-dot supports and SACs with a modified microenvironment of $Cu-N_2-O_2$, which was confirmed with an EXAFS fitting curve (Figure 4a) and showed an ultrahigh faradaic efficiency (FE) of 78% toward methane production through electrochemical conversion from CO_2 (Figure 4b).[76] The introduction of oxygen ligands on the center Cu single-atom site and partial-carbonization strategy during the synthesis process offered a chance to modify the electronic structure of the center Cu atom and hence lowered the overall thermodynamic barrier in associating with intermediates during the CO_2 reduction pathway to CH_4 (Figure 4c). Moreover, high selectivity with suppressed competing HER to maximize CH_4 production was enabled by the properly elevated H_2 energy barrier resulting from the fine-tuned electronic structure of Cu active sites (Figure 4d).

Ju et al. demonstrated the trends in the CO_2 to CO electrocatalysis of metal- and nitrogen-doped porous carbons containing catalytically active $M-N_x$ moieties (M = Mn, Fe, Co, Ni, Cu).[77] From their computationally calculated and experimentally obtained catalytic reactivity, CO turnover frequencies, and CO faradaic efficiencies (FE_{CO}), Fe−N−C and especially Ni−N−C catalysts have huge potential to rival Au- and Ag-based catalysts based on reactivity-selectivity descriptors. Specifically, Fe−N−C and Ni−N−C catalysts clearly acted as highly promising catalysts for selective CO production. However, the maximum FE_{CO} was obtained at a smaller overpotential on Fe−N−C (V_{RHE} = −0.55 V, FE_{CO} = 65%) than on Ni−N−C (V_{RHE} = −0.78 V, FE_{CO} = 85%) (Figure 4e). Thus, atomic-scale mechanistic understanding of potential-dependent CO and hydrocarbon selectivity from the $M-N_x$ moieties was revealed and could be utilized for the further rational design of efficient and superior electrocatalysts.

Also, Gu et al. reported atomically dispersed Fe atoms embedded on a pyrrolic N-doped carbon support that efficiently reduce CO_2 to CO without using expensive gold.[23] This nonprecious metal catalyst showed modest activity toward electroreduction of CO_2 with an increased oxidation state of single-atom Fe active sites from +2 to +3. Coordinated N atoms were responsible for this elevated oxidation state and resulted in superior activity, showing that Fe^{3+} sites offer faster CO_2 adsorption and weaker CO adsorption than that of conventional Fe^{2+} sites.[23] In addition, Zhang et al. synthesized a catalyst with a Pd dimer (Pd_2) embedded on the carbon support and confirmed the CO_2RR catalytic performance with FE_{CO} of 98.2% at −0.85 V versus RHE, which was a higher CO selectivity compared to FE_{CO} of 80% and 65% for a Pd single atom or Pd nanocluster embedded on the carbon support, respectively.[78] In addition, Zhu et al. recently revealed that neighboring Zn and Co atoms located in pyridine N-doped carbon showed unprecedented CO_2 electroreduction to CO.[34] The neighboring effects of Zn and Co atoms adjusted the intermediate bonding strengths and the reaction pathway that resulted in increased FE_{CO} of 93.2% at −0.5 V versus RHE. Further investigations unveiled the modified reaction mechanisms and confirmed that *COOH intermediate bonding on Zn sites became stronger, which accelerated the CO production.

Nitrogen Reduction Reaction

The electrochemical nitrogen reduction reaction (NRR) is one of the most promising routes for nitrogen fixation and ammonia production, which is beneficial to the industrial fields related to fertilizers or chemicals. However, the low FE toward NH_3 and the large overpotential in the NRR process have distinctly impeded further development of the NRR. To fully unleash the latent potential in electrocatalytic NRR, advanced SAC electrocatalysts with rationally designed active sites combined with diverse support materials have recently the attracted attention of researchers for their unprecedented catalytic activity and selectivity resulting from the unique structural and electronic features of multicomponent SACs. Since the electrocatalytic NRR has a more complex reaction pathway than other electrochemical reactions like HER, OER, and ORR, the structure−activity relationships should be clearly revealed for the rational design of efficient NRR electrocatalysts.

With the help of DFT calculations, Liu et al. constructed a combinational set of 20 different transition metal atom centers anchored on three different nitrogen-doped carbon supports to figure out the intrinsic activity trends in NRR and improve the NRR activity of SACs.[79] As a result, a nitrogen adatom adsorption energy was responsible for the overall NRR activity trends and proved to be related to the scaling relations for the adsorption of intermediates. This work predicted the catalysts of Ru single atoms embedded in graphitic carbon nitride (Ru@g-C_3N_4) as the best performing electrocatalysts for NRR, since their activity was located at the top of the activity related volcano-like plot that demonstrated the relationship between adsorption energy of nitrogen adatom and the thermodynamic limiting potential.

The theoretically promising Ru single atoms dispersed in nitrogen-doped carbon were experimentally verified by Geng et al., achieving a FE of 29.6% for NH_3 production with a partial current density of −0.13 mA cm^{-2} and record-high NH_3 yield rate.[80] The discovery of this superior NRR electrocatalyst clearly encourages the synergetic cooperation of computational predictions and experimental validations toward further advances in NRR electrocatalyst design and development. There is still much room for additional improvement such as replacing the previously explored Ru single-atom center with other single-atom elements or modulating the atomic neighboring coordination of the single-atom metal centers,[81−83] since the combinational diversity and unexplored latent potentials in multicomponent SACs are immense.

GENERAL SYNTHESIS METHODS FOR SACS

Controllable synthesis of SACs with the desired structures and properties is the most important step in developing multicomponent SACs. Appropriate synthesis methods to manipulate and arrange the atoms at the atomic scale can benefit SACs to achieve ultrahigh metal atom utilization efficiency, hence reducing the usage of the metal resources and the

https://doi.org/10.1021/acsmaterialsau.1c00041
ACS Mater. Au 2022, 2, 1−20

economic costs, or disperse identical active sites for definitive characterization of structure−activity relationships. One of the most widely used materials in synthesizing SACs is MOFs composed of metal ions or clusters and the bridge role of organic linkers. Because of their porous crystalline structure, high specific surface, and controllability at the atomic scale via internal pore area, MOFs are promising materials in preparing SACs with improved catalytic activity[84] or as neighboring assistants of SACs by controlling the coordination environment at the atomic level.[85] However, MOFs are not the only choice in SAC preparations since there are plenty of other approaches that do not depend on the usage of MOFs.[86,87] In this part of the Review, we will summarize some general synthesis strategies for SACs, such as pyrolysis, atom deposition, and facile synthesis, including solution phase synthesis, solvothermal synthesis,[88] and microwave synthesis,[89] which can be potentially expanded to multicomponent SAC preparation methods.

Pyrolysis

Pyrolysis has been widely investigated as a common synthetic strategy to fabricate atomically dispersed SACs at elevated temperatures over 703 K to decompose materials thermally. In particular, treatment with MOF-assisted pyrolysis results in the fabrication of various unique porous nanostructures including hollow, core−shell, and yolk−shell structures; these structures have received attention for their superior properties such as low density, excellent catalytic stability, and high surface volume of a core surrounded with a shell for enhancing the catalytic performance of the material.[90] To capture more single atoms, zeolitic imidazolate frameworks (ZIFs) have been considered to be a single-atom precursor candidate owing to the abundance of N species, controllable atomic coordination number, and high specific surface area where a single atom can be anchored on the defect sites after the high temperature pyrolysis process.[91]

Li et al. recently reported monodispersed cobalt single atoms embedded in a conductive nitrogen-doped carbon nanosheet (CoSA-N-C) with a high cobalt loading over 15.3 wt % through the salt-template method with pyrolysis, derived from a cobalt-based zeolitic imidazolate framework (ZIF-67) precursor for lithium−sulfur battery anode materials.[92] The synthetic process through pyrolysis was started from potassium chloride (KCI) particles with the growth of ZIF-67 through the coordination of a cobalt (II) metal ion and 2-metyhlimidazole organic linker at 70 °C. The ZIF-67@KCI composite was pyrolyzed under an argon atmosphere at 750 °C for 2 h and then washed with the hydrochloric acid solution to obtain the final CoSA-N-C. Also, the TEM image confirmed that the as-synthesized CoSA-N-C has a two-dimensional nanosheet morphology. Additionally, the homogeneous distribution of C, N, and Co elements was observed by the energy dispersive X-ray mapping images of CoSA-N-C. The aberration-corrected high angle annular dark-field scanning transmission electron microscopy (HAADF-STEM) image can elucidate that many bright dots with a red circle correspond to a cobalt single-atom site dispersed uniformly on a carbon support.

Moreover, derivation from a ZIF to synthesize single-component SACs could also be applied to preparing SACs with multicomponent active sites that are expected to show unexpected synergistic effects due to the cooperative interactions between the components in the active sites and their surrounding environment.[93] For example, Yan et al. reported a Zn and Ni bimetallic ZIF-8 with different molar ratios of zinc to nickel to confirm the coordination number through a pyrolysis method,[94] with delicate fabrication procedures for the Zn/Ni bimetallic ZIF-8. Prepared with different concentrations of Zn/Ni bimetallic ZIF-8s, denoted as Zn_xNi_y ZIF-8, they were pyrolyzed under an Ar atmosphere. Different temperatures and holding times of pyrolysis were studied; C-ZIF-8, C-Zn_2Ni_1 ZIF-8, and C-Zn_1Ni_1 ZIF-8 were obtained at 1000 °C for 4 h, and Zn_1Ni_4ZIF-8 was obtained at 900 °C for 10 h to sustain the high loading formation of Ni content during pyrolysis.

In addition, low-resolution HAADF-STEM images with energy-dispersive X-ray spectroscopy (EDX) demonstrate atomically dispersed elements C, N, Ni, and Zn in C-Zn_1Ni_4 ZIF-8. Moreover, high-resolution TEM (HRTEM) images and high-resolution HAADF-STEM images of C-Zn_1Ni_4ZIF-8 contributed to classifying the porous graphitic carbon and atomic dispersion of metal species. Furthermore, to fabricate ideal multicomponent SACs, Lin et al. designed cobalt phthalocyanine anchored in Fe−N−C through a sequential pyrolysis and impregnation method assisted by a ZIF-8 precursor developing a synergetic effect of interaction between the cobalt and iron metal active site for the reduction of CO_2.[26] In addition, Fu et al. demonstrated Ir_1Mo_1 multicomponent SACs synthesized through a sequential adsorption and pyrolysis of organometallic precursors which exhibited a more favorable chemoselectivity in the hydrogenation of 4-nitrostyrene to 4-vinylaniline compared to single metal Ir_1 or Mo_1 SACs, respectively.[95] Also, multicomponent SACs with the reduced amount of the noble metal atom usage can be fabricated via the pyrolysis method. For example, Zhang et al. successfully synthesized a locally dispersed Pt−Co embedded on nitrogen-doped carbon (Pt−Co@NC) with a successive pyrolysis at 850 °C and electrochemical activation.[96] Therefore, pyrolysis is one of the most facile synthesis strategies for multicomponent SACs, which provides enough thermal energy to activate and transform the morphologies and the compositions of the target materials in the desired directions.

Atomic Layer Deposition

For the successful fabrication of SACs, atomic layer deposition (ALD) is another widely used synthesis method.[97,98] As the frontier of chemical vapor deposition, ALD is a powerful technique that relies on self-limiting chemical and molecular-level surface reactions of vapor-phase reactants and a solid surface by controlling thickness at the atomic level has several advantages including highly uniformly distributed single atoms,[99] superior conformity, and chemical selectivity of the solid surface for preparing heterogeneous SACs by downsizing the particle size to the nanometer level.[97−100] Depositing atomic layers on the highly conductive materials such as graphene,[101] N-doped graphene,[102] graphene oxide,[103] C_3N_4,[104] and MOF derived porous carbon have attracted much attention as solid substrate candidates owing to their extraordinary crystalline structures, superior electrochemical properties, and defect sites to increase catalytic activity.[105] For example, Kim et al. achieved a high yield of hydrogen gas sensors using selective functionalization of Pt single atoms deposited on defect sites of graphene.[101]

Fang et al. recently introduced atomically dispersed Pt single atoms on a Uio-66-NH_2 derived N−C framework via ALD as a electrochemical hydrogen evolution reaction catalyst.[106] As

https://doi.org/10.1021/acsmaterialsau.1c00041
ACS Mater. Au 2022, 2, 1−20

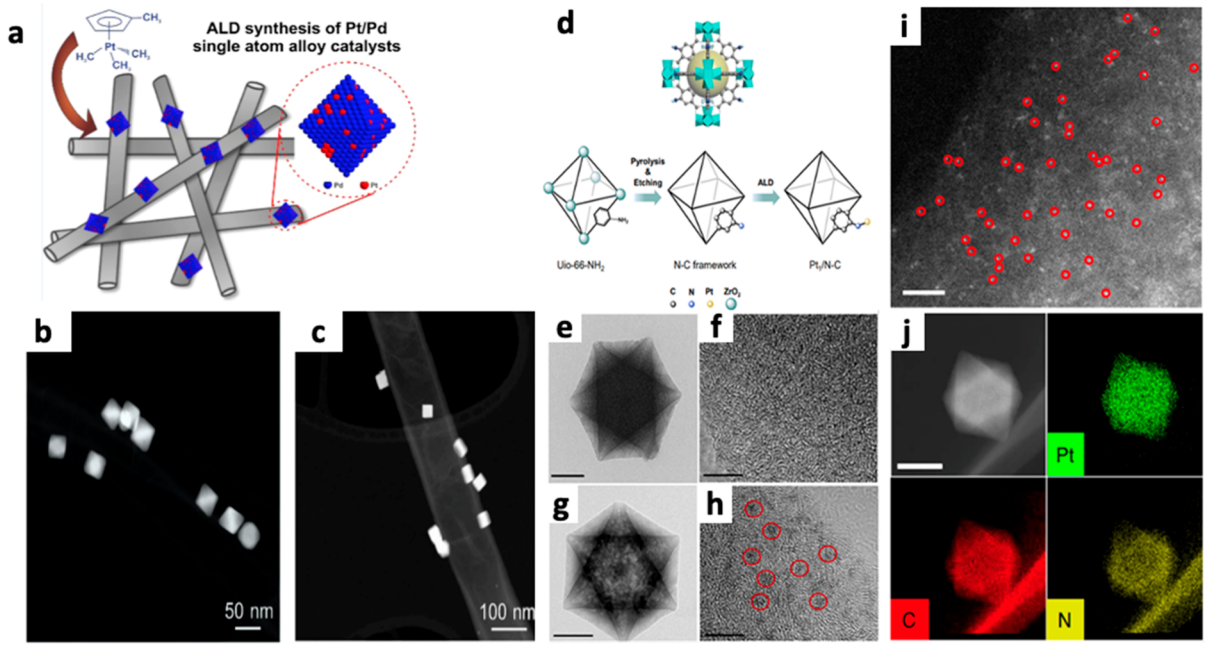

Figure 5. (a) Preparation process of Uio-66-NH_2 structure and Pt_1/N−C. (b, c) Low magnification TEM images of Pt ALD on a Uio-66-NH_2 derived N−C frame and on a Uio-66 derived C frame, (d) schematic of the ALD process in preparing Pt_1/N−C, and (e, g) corresponding high magnification TEM images, respectively. (f) HAADF-STEM images and (g, h) corresponding EDX elemental mapping images for C, N, and Pt in Pt_1/N−C. (a−h) Adapted with permission from ref 106. Copyright 2020 Nature Publishing Group. (i, j) Low magnification STEM images of the Pt/Pd heterogeneous-single-atom particles. Reproduced from ref 111. Copyright 2019 American Chemical Society.

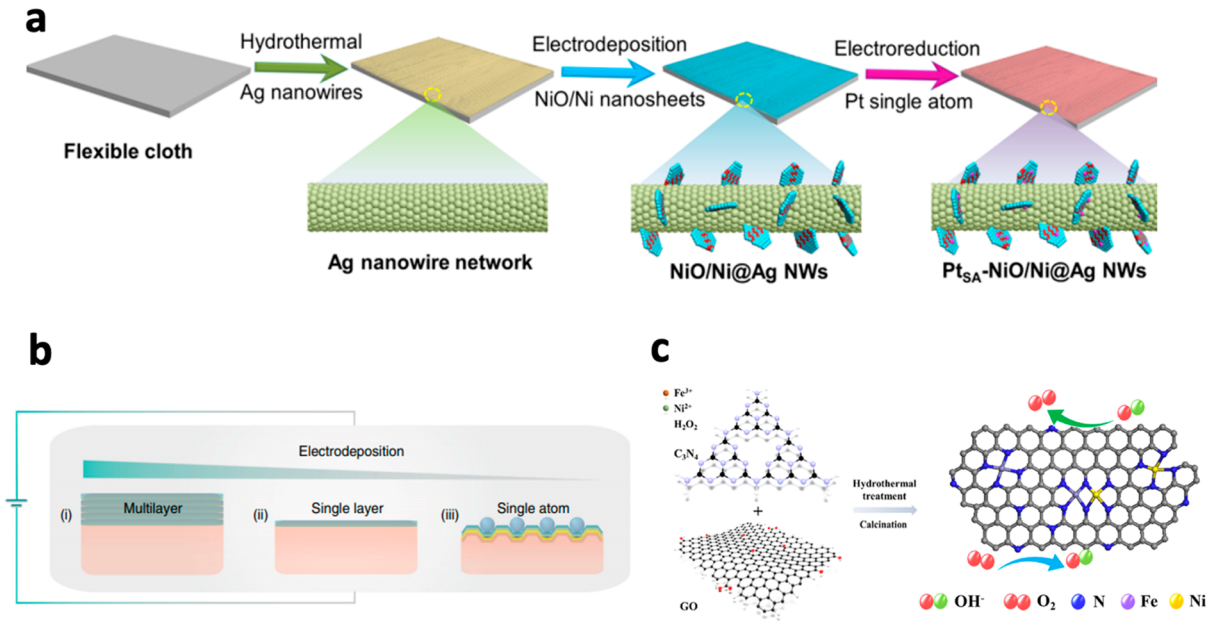

Figure 6. (a) Fabrication process of Pt single atom integrated with NiO/Ni nanosheets on Ag nanowires via electrodeposition. Adapted with permission from ref 58. Copyright 2021 Nature Publishing Group. (b) Schematic illustration of atomically dispersed metal catalyst (ADMC) preparation process using an electrodeposition method. Adapted with permission from ref 123. Copyright 2020 Nature Publishing Group. (c) Schematic illustration of synthesizing a Fe/Ni(1:3)-NG catalyst. Adapted with permission from ref 133. Copyright 2021 Elsevier.

illustrated in Figure 5a, Pt/N−C fabrication started with synthesizing the Uio-66-NH_2 precursor using a $ZrCl_4$ metal ion and H_2BDC-NH_2 organic linker dissolved in DMF and acetic acid (HAc). Then, using the as-prepared Uio-66-NH_2, Pt/N−C SAC was prepared by ALD with a time sequence of 80, 120, 60, and 120 s to expose the trimethylcyclopentadienyl-platinum (MeCpPtMe3) precursor and O_2. As a result, a well-defined MOF structure and uniformly deposited Pt single atoms with a local coordination environment into the N−C framework of the MOF were successfully fabricated. To confirm the Uio-66 derived carbon framework integrated with Pt atoms, low magnification TEM (Figure 5b, d) and corresponding high magnification TEM images (Figure 5c, e) proved the that N−C framework provides efficient prevention from the aggregation of Pt under the ALD process. Furthermore, the HAADF mode of the STEM image

https://doi.org/10.1021/acsmaterialsau.1c00041
ACS Mater. Au 2022, 2, 1−20

demonstrates that Pt single atoms in Pt/N−C are uniformly distributed on the N−C framework (Figure 5f), and EDX element mapping of C, N, and homogeneous distribution of Pt was also exhibited (Figure 5g, h). Thus, deposited platinum-based single atoms via ALD had been applied in various applications, including not only selective hydrogenation and dehydrogenation[107] but also NO reduction,[108] electrochemical catalysts,[109] and CO oxidation.[110]

Furthermore, Zhang et al. significantly developed the electrocatalytic activities for OER and HER through Pt and Pd heterogeneous single-atom alloys using the ALD process due to the synergistic effect of those metal interactions.[111] Zhang employed different diameters of nitrogen-doped carbon nanotubes (NCNTs) as the substrate by ultrasonic spray pyrolysis to avoid the aggregation of Pt atoms when deposited on Pd/NCNT. Following several ALD cycles, high purity N_2 was used as a carrier gas and MeCpPtMe3 was used as a precursor to deposit on the shape-controlled Pd/NCNTs. Low magnification STEM images in Figure 5i and j show a well-defined octahedral Pt/Pd heterogeneous single atom and cubic shape of Pt/Pd particles on NCNTs, respectively. Recently, Zhang et al. also prepared a high-quality of Pt−Ru multidimer structure via the ALD process. Compared to fabricating general SACs, designing multicomponents SAC under the ALD process exhibited excellent properties in terms of stability, good electrocatalytic activity, and high-quality atomic structure by sophisticatedly controlling the coordination number.[37]

Electrodeposition

Electrodeposition (ED) is an electrochemical deposition process applied for surface modification; it is an important technology for fabricated nanostructures and has potential in industrial applicability due to its rapid process route,[112] classification,[113] size-controlled ability,[114] low cost, and high purity for the production of SACs.[115,116] Bose et al. reported an unary oxide (CeO_x)/heterogeneous bimetallic-hydroxide (NiFe−OH) composite on porous nickel foam for the efficient catalysis of water oxidation under a two-step facile ED process by achieving long-term stability over 80 000 s and a low Tafel slope of 43.2 mV dec^{-1}.[117] To improve the catalytic activity of electrochemical CO_2 reduction, Qiu et al. introduced a pulse-electrodeposition method for depositing Cu particles to have high energy facets of a smooth surface on carbon paper.[118] Moreover, ED is a widely applied strategy for fabricating stable and efficient SACs to prevent metal single atoms from aggregating, an obstacle to unambiguously identifying the uniformly dispersed particles.[119,120]

Zhou et al. prepared a heterogeneous structure of Pt_{SA}−NiO/Ni SAC, using the ED method, as a HER catalyst by enhancing the binding abilities to hydroxyl ions and hydrogen (Figure 6a).[58] The synergy effects of a 3D Ag nanowire and 2D heterogeneous Ni/NiO nanosheet consisting of anchored Pt single atoms via two-step ED under −1.2 V versus SCE (saturated calomel electrode) for 200 s show significantly outstanding catalytic performance. Moreover, the under-potential electrodeposition (UED) technique, a surface-limited method to fabricate highly uniformed monolayers on the substrate surface, was properly used to prepare atomically dispersed SACs.[121,122] For instance, Shi et al. first explored the fabrication strategy of atomically dispersed SACs by conventional UED at a more positive potential than the equilibrium potential.[123] They synthesized Pt_{SA}/MoS_2 by exchanging Cu atoms with Pt atoms deposited on a molybdenum disulfide (MoS_2) support, which is a high electrical conductivity material of the two-dimensional transition metal dichalcogenides (TMD) class, at more a positive potential of a galvanic system of UED (Figure 6b).

Hydrothermal Treatment

As an ideal bottom-up synthetic method, the hydrothermal treatments with thermochemical conversion process had attracted enormous enthusiasm due to its versatile strength in preparing distinctive nanostructured SACs involving nanoflowers,[124] nanorods,[125] nanosheets,[126] hierarchical structures,[127] and even heterogeneous structures.[128,129] For example, single ruthenium atoms embedded with high 2H phase MoS_2 had nanoflower or nanosheet structure (Ru@2H-MoS_2) under a hydrothermal reaction at 80 °C for 2 h, which was introduced as an efficient HER catalyst by Wang et al.[130] Starting from a cobalt metal source and nitrogen-doped active carbon, Zhong et al. prepared single Co atoms anchored on the carbon support through a two-step hydrothermal process at a high temperature over 600 °C for fabricating the bifunctional electrochemical catalyst. Furthermore, Fei et al. reported a facile hydrothermal process assisted by H_2O_2 for fabricating an atomically distributed transition metal integrated into nitrogen-doped graphene, denoted as M-NHGFs, for a heterogeneous tunable electrochemical SAC.[64] Adding H_2O_2 aqueous solution into graphene oxide during hydrothermal treatment, which is called the oxidative-etching process, led to the graphene having porous in-plane holes which can improve mass transport activity via rich defective sites.[131,132] Additionally, to prevent aggregation of the metal site of multicomponent SACs and improve the intrinsic activity, the hydrothermal method was a rational synthetic method to manifest the synergistic effects of different neighboring single-atom elements. For example, Yang et al. introduced controllable oxygen coordinated tungsten−molybdenum anchored in N-doped graphene through a facile two-step hydrothermal method for a HER catalyst having a remarkable stability in terms of strong covalent interactions between W−Mo dual atoms and N-doped graphene, which can bring an unexpected synergetic effect.[56] In addition , Ma et al. synthesized bifunctional catalysts for OER and ORR with atomically dispersed FeN_4 and NiN_4 in nitrogen doped graphene by hydrothermally treating the mixture of different metal precursors (Figure 6c), which were endowed with great potential to be suitable electrode catalyst materials for practical ZABs.[133]

CHARACTERIZATION TECHNIQUES FOR SACs

Precise and effective characterization of SACs is critical for the fundamental understanding of SACs and unveiling their exact mechanisms. To elucidate SACs at the atomic scale, the development of powerful characterization techniques plays a crucial role in investigating the isolated single atoms anchored on substrates and their neighbor coordination, hence confirming the existence of the atomic active sites and the dynamic behavior of catalysts during reaction processes, which is more complex for multicomponent SACs.[134,135] X-ray assisted characterizations are also essential to reveal and understand the fundamental information embedded in SACs, providing critical physicochemical characteristics, electronic structures, oxidation states, and chemical bonding between multicomponent active sites and the intermediates in electrochemical reactions.

https://doi.org/10.1021/acsmaterialsau.1c00041
ACS Mater. Au 2022, 2, 1−20

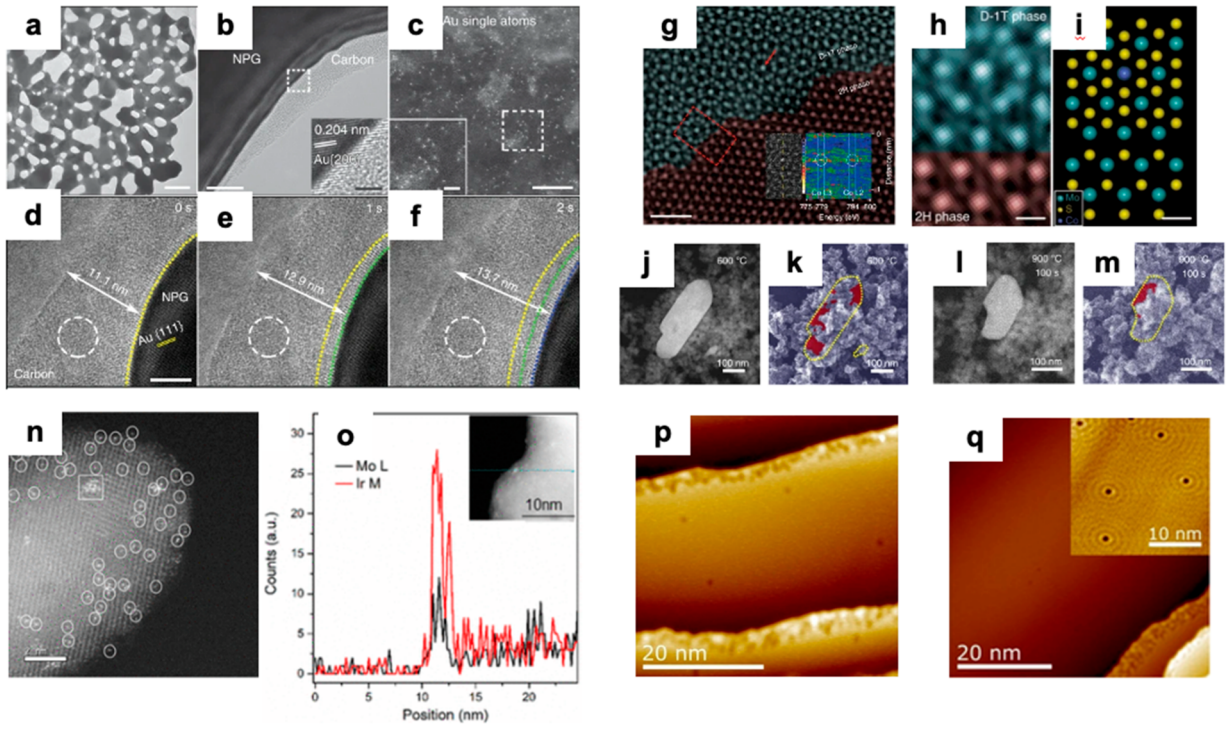

Figure 7. (a) TEM and (b) HRTEM images of an NPG sample after the reaction. (c) HAADF image of a carbon region on the NPG sample. Insets in (b) and (c) are the close-up views of the boxed regions, respectively. (d–f) HRTEM images at three different moments during the reaction on a surface region with positive curvature. The images have the same scale bar. The moment in (a) is defined as 0 s. The yellow, the green, and the blue dashed lines indicate the positions of the surface at 0, 1, and 2 s, respectively. The white dashed circles denote the positions of a randomly selected carbon region, and the arrows indicate the thickness of the amorphous carbon at 0, 1, and 2 s. (a–f) Adapted with permission from ref 143. Copyright 2020 Nature Publishing Group. (g) Aberration-corrected HAADF-STEM image of SA Co-D 1T MoS_2, showing the obvious junction between SA Co-D 1T MoS_2 (dark cyan) and pristine 2H MoS_2 (red). Inset shows the HRTEM and EELS spectrum of SA Co-D 1T MoS_2 (scale bar: 1 nm). (h) Enlarged HAADF-STEM image in the red square area of (b) (scale bar: 2 Å). (i) Theoretical modeled and simulated STEM images using QSTEM simulation software (scale bar: 2 Å). (j, l) In situ AC-HAADF-STEM images and (k, m) corresponding images of a RuO_2+MAFO physical mixture after calcination at 600 and 900 °C (100 s) under flowing O_2 (2 mL min^{-1} and 3.5 Pa). (g–m) Adapted with permission from ref 144. Copyright 2019 Nature Publishing Group. (n) STEM image of Ir_1Mo_1/TiO_2. White circles highlight single Ir or Mo atoms, and white squares contain clusters. (o) LS-EDS of a selected cluster from Ir_1Mo_1/TiO_2 (inset shows the area at which the line scanning was performed). (n, o) Reproduced from ref 95. Copyright 2021 American Chemical Society. (p, q) LT-STM images showing the formation of RhCu(111) multicomponent SACs. (p) RhCu alloy with Rh sites imaged as depressions showing isolated Rh atoms in brims above step edges as well as in terraces. (q) Dense brims of isolated Rh sites above a large lower terrace demonstrating how underlying terraces act as catchment areas for incoming Rh which place exchange at step edges into the upper terrace. Inset shows atomic resolution of Rh sites. (p, q) Adapted with permission from ref 149. Copyright 2020 Wiley.

Electron Microscopy

High-resolution techniques like TEM, HRTEM, and aberration-corrected HAADF-STEM can provide an intuitive and systematic construction of SACs by breaking the practical resolution limitation and hence distinctly observe the existence of the multicomponent active sites.[33,136] Higher atomic number elements typically utilized for SACs can be sensitively detected on the substrate by their contrast difference from electron beam scattering. Since electrons are more scattered at a high angle in TEM by larger electrostatic interactions between the electrons and nucleus, annular dark field images produced by HAADF-STEM mode can clearly show isolated single atoms anchored on substrates.[137,138] Aberration-corrected TEM techniques have substantial enhancements in analyzing nanoparticles and SACs and produce in situ/operando characterization of catalytic materials. The in situ/operando TEM techniques lead to further investigation of the dynamic behavior of catalysts in the reaction process and determination of the reaction intermediates or catalytic active sites.[139−142] Xi et al. revealed the dynamic methane pyrolysis process of Au single atoms and Au nanoporous cocatalysis using in situ TEM with high spatial-temporal resolution.[143] TEM, HRTEM, and HAADF images of nanoporous gold (NPG) after methane pyrolysis reaction clearly show that the pores in NPG became larger and amorphous carbon was formed on the surface of all Au ligaments (Figure 7a–c). The HAADF image noticeably shows that a significant amount of heavy metal (Au) SACs was produced in the amorphous carbon, indicating the release of Au SACs from NPG during the methane pyrolysis process. In order to certify this conclusion, HRTEM images at three different moments of methane pyrolysis were obtained (Figure 7d–f). The high temporal resolution of TEM and STEM made it possible to monitor the dynamic motion of Au crystal surfaces. In situ analysis showed that the thickness of the amorphous carbon gradually increased, which indicates that the methane pyrolysis occurred on the surface during the measured time. As the reaction continued, the diameter of the NPG ligaments decreased due to the intensive release of Au SACs from Au NPG.

Qi et al. reported a highly efficient and stable HER catalyst consisting of an interface atomic cobalt array covalently bound

https://doi.org/10.1021/acsmaterialsau.1c00041
ACS Mater. Au 2022, 2, 1–20

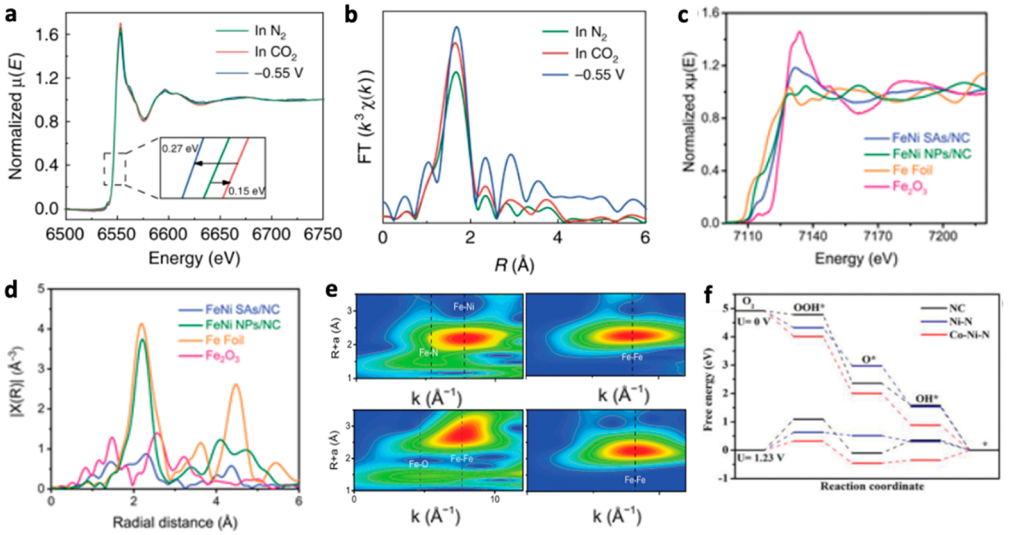

Figure 8. (a, b) XANES and EXAFS spectra at the Mn K-edge of Mn−C_3N_4/CNT under various conditions. Adapted with permission from ref 150. Copyright 2020 Nature Publishing Group. (c) Fe K-edge XANES spectra, (d) FT-EXAFS spectra, and (e) WT-EXAFS of the Fe K-edge of FeNi SAs/NC, FeNi NPs/NC, Fe foil, and Fe_2O_3 from the top right side in a clockwise direction. (c−e) Adapted with permission from ref 151. Copyright 2021 Wiley. (f) Free energy diagram of ORR pathways at 0 and 1.23 V on NC, Ni−N, and Co−Ni−N. Adapted with permission from ref 25. Copyright 2019 Wiley.

to distorted 1T MoS_2 nanosheets.[144] They elucidated the atomic dispersion of cobalt and the phase transition of MoS_2 through HAADF-STEM with atomic electron energy loss spectroscopy (EELS) methods. The obvious interface was generated between pristine 2H MoS_2 and the disordered structure of Co-D 1T MoS_2, (Figure 7g, h) and further investigated via theoretical modeling (Figure 7i). The inset in Figure 7g shows the EELS data of Co SACs, exhibiting Co peaks at 779 and 794 eV, and each corresponds to Co L3 and Co L2, respectively. Also, Liu et al. demonstrated that the Ru SACs were thermally stable with high NO_2 decomposition ability because of a strong covalent metal−support interaction between RuO_2 and $MgAl_{1.2}Fe_{0.8}O_4$(MAFO).[145] They investigated and visualized the dispersion process of Ru SACs from composite materials of RuO_2 and MAFO, namely, RuO_2+MAFO, through aberration-corrected HAADF-STEM and simultaneous secondary electron (SE) detection. From in situ aberration-corrected HAADF-STEM images and corresponding SE images of RuO_2+MAFO after different calcination processes (Figure 7j−m), while the morphology and size of the RuO_2 aggregates were kept at a temperature below 900 °C, they shrank by approximately 50% in all dimensions in 100 s at 900 °C.

Also, SE imaging showed that the RuO_2 was partially embedded in the MAFO support and immobilized during the calcination. This information from in situ electron microscopy could derive the mechanism of Ru SAC formation as breaking away from the static RuO_2 and diffusing across the MAFO surface until it is trapped by a covalent metal−support interaction.

Since multicomponent SACs have the virtue of enhanced activity and selectivity through the flexible combinations of different types of single atoms, they recently emerged as new a SAC development strategy with the synergistic effect of various active sites and the optimization of geometric and electronic structures.[24,47,146] Advanced electron microscopy techniques are necessary for the accurate characterization of different component materials of atomic scale. Aberration-corrected HAADF-STEM can distinguish pairs of atoms through high selectivity in Z contrast. High-resolution scanning tunneling microscopy (STM) can also be an effective method for the precise surface observation of multicomponent SACs. Since STM can image surfaces with a lateral resolution of 0.1 nm and a depth resolution of 0.01 nm, individual atomic structure and conductive surface phenomena can be detected more accurately.[95,135,147]

X-ray Assisted Structure Identification

While highly technical electron microscopy gives direct and intuitive evidence for the atomic level environment, X-ray absorption spectroscopy (XAS) can provide the critical physicochemical characteristics of SACs. EXAFS, XANES, and operando/in situ XAS are widely utilized to reveal the geometric and electronic structures of SACs, investigating the chemical bonding features, oxidation states, and coordination environment of SACs.[42,141,148]

Fu et al. demonstrated multicomponent SACs of Ir_1Mo_1/TiO_2 exhibiting very enhanced catalytic chemoselectivity compared with the single-component counterparts and Mo_1/TiO_2 in the hydrogenation of 4-nitrostyrene (4-NS) to 4-vinylaniline.[95] The structure of uniformly dispersed discrete single atoms Ir and Mo on TiO_2 could be efficiently characterized through aberration-corrected HAADF STEM investigation. A small number of bright clusters with a diameter less than 1 nm in Figure 7n indicates the Ir_1Mo_1 multicomponent SACs. In order to clearly distinguish Mo atoms from Ir atoms, linear-scanned energy-dispersive X-ray spectroscopy (LS-EDS) was conducted on some clusters, showing the coexistence of Mo and Ir elements (Figure 7o). Hannagan et al. also reported the usage of low-temperature STM (LT-STM) to interpret the atomic structure of RuCu multicomponent SACs, the behavior of the common probe molecule CO, and the alloying process of Ru into a Cu(111) S^4C crystal (Figure 7p).[149] Ru atoms mainly lie in brims along step edges, and some of them also are scattered throughout the terraces of Cu surfaces. In Figure 7q, denser brims above larger

https://doi.org/10.1021/acsmaterialsau.1c00041
ACS Mater. Au 2022, 2, 1−20

terraces mean that the terraces acted like a catchment area for incoming Rh atoms.

Feng et al. reported a Mn single-atom catalyst with a Mn−N_3 site embedded in graphitic carbon nitride, exhibiting a 98.8% CO faradaic efficiency with a high current density of CO of 14.0 mA cm^{-2} at a low overpotential of 0.44 V in an aqueous electrolyte.[150] Through the in situ XANES and EXAFS investigations (Figure 8a, b), they determined the performance factor of the catalyst as the Mn−N_3 site on which CO_2 is adsorbed, activated, and converted, hence leading to the decreased free energy barrier in the formation of the key intermediate COOH*. Yu et al. developed Fe−Ni multicomponent SACs embedded in a nitrogen-doped carbon matrix (FeNi SAs/NC), having exceptional activity in OER and ORR processes.[151] XANES for FeNi SAs/NC and FeNi nanoparticles (NPs)/NC (Figure 8c) indicates that the average valence state of Fe in FeNi SAs/NC is higher than that in FeNi NPs/NC. Also, the variation trend of the white line intensity in XANES data indicates that the increased white line intensity is relevant to the increased percentage of single-atomic and proposed single-atomic structures. By investigating the bonding coordination through K^3-weighted Fourier transform (FT)-EXAFS spectra in the R-space (Figure 8d), it could be concluded that no Fe−Fe nanoparticles exist in FeNi SAs/NC. Wavelet transform (WT)-EXAFS for Fe K-edge in K-space (Figure 8e) could aid in distinguishing the adjacent properties of the metal atoms. The WT signals of metal−metal bonds are observed in the contour plots of FeNi SAs/NC, FeNi NPs/NC, Fe foil, and Fe_2O_3, and the peak intensity of the Fe−N signal is located at $k \approx 5$ $Å^{-1}$, close to that of Fe−O in Fe_2O_3, consistent with the Fe K-edge FT-EXAFS results.

DFT Calculations

Computational modeling using DFT can be a powerful method to investigate the insightful mechanism of SAC reactions, especially in revealing the cooperative effect of different metals in multicomponent SACs.[152−154] Han et al. unveiled the synergistic effect of Co−Ni SACs in the ORR process.[25] Downhill free energy pathways of NC, Ni−N, and CO−Ni-N in ORR at $U = 0$ V substantiate that all electron transfer steps can proceed spontaneously (Figure 8f). By comparing the limiting potential for ORR, the ORR capability trend follows the order of NC < N−N < Co−Ni−N. Also, through analyzing the rate-determining step (RDS) at an equilibrium potential of 1.23 V, while the RDS on NC and Ni−N is the hydrogenation of molecular O_2, the RDS of Co−Ni−N is the protonation of OH* by the large decrease in the largest uphill value, manifesting the facilitation role of bimetallic Co/Ni sites in the ORR process.

Furthermore, DFT calculation can quantitatively compute meaningful values like adsorption energy of the specific adsorbate during an electrochemical reaction, which is expected to correlated with the catalytic activity under the intrinsic scaling relationships.[155] The predicted activity information can be a valuable tool to accelerate the discovery of unexplored superior electrocatalysts and to guide the rational design of catalysts with desired properties. For example, complex intermediates and numerous reaction pathways in electrocatalytic CO_2RR are the main obstacles to efficiently optimize the catalysts, and Gong et al. developed a descriptor that was highly correlated with the catalytic activity of metal single atoms embedded in nitrogen-doped carbon supports.[156] The descriptor consisted of the valence electron number of the metal center atoms, the radius of the metal ions, and the electronegativity of the central metals successfully representing the topological, bonding, and electronic structures of the catalytic centers, and the volcano-shaped relationships between the descriptor and catalytic activity were established to predict that Ti and Co might be the best metal center atom of the SACs for CO_2 reduction. With the help of DFT calculation, activity prediction and catalyst discovery for other electrochemical reactions have been successful, such as the scaling relations between the thermodynamic limiting potential and nitrogen adatom adsorption energy for NRR[79] or the relationships between the binding energy of *OOH and the intrinsic activity via two-electron or four-electron pathways for ORR.[71]

CHALLENGES AND FUTURE DIRECTIONS

Although multicomponent SACs have several advantages, such as an ultrahigh atomic utilization efficiency, tunability of the active sites for advanced electronic structures, charge transport, and synergistic effects between active metal centers and the modified coordination or the support materials, that are beneficial for catalysis in various electrochemical reactions, the engineering of multicomponent SACs is still in its infancy, and various remaining challenges must be overcome for successful industrial implementations. For example, nonuniform and low loading of active sites in SACs is one of the main obstacles for efficient utilization of atomic metals and precise characterization for the overall surface of catalysts. Also, poor stability under realistic working conditions is another problem and must be solved by enhanced stabilization via stable anchoring of SACs on supports. Most of the synthesis methods presented in this Review to prepare SACs are limited to laboratory conditions. Therefore, synthesis methods should be economically scalable for large-scale applications of multicomponent SACs in the industry. In addition, the fundamental catalytic dynamics of SACs are still ambiguous and barely understood, which is even more challenging for multicomponents,[146,157,158] leading to an urgent need for advanced in situ/operando spectroscopic techniques to confirm the surface morphology during catalysis and to gain insight into structure−activity relationships. Although the limitations in resolution of electron microscopy have been broken through powerful techniques like HADDF STEM or aberration corrected TEM and STEM, distinguishing different types of nearby multicomponent metal SACs having similar Z values is the still remaining obstacle.[159] Also, HADDF STEM only provides images of restricted regions and it can miss the actual active sites where catalytic reactions occur. Explicit analyses of similar atomic number elements with more a developed scale of the EDS mapping system and the enlarged scope of measuring sites are needed for identifying various dynamics and mechanisms in multicomponent SACs. The EXAFS methodology also retains the issue of not being sensitive enough to separate SACs from coexisting compositions like nanoparticles or clusters. Advanced characterization strategies and computational simulations should be collaborative to reveal structures and dynamics of the multicomponent active sites during catalytic reactions and unveil the catalysis mechanisms of the multicomponent SACs for further improvement and deeper insights.

Recently, various approaches have been reported to handle the challenges mentioned above. For example, Xia et al. demonstrated transition metal (TM) SACs with comparably high loading by using a graphene quantum dot interweaved

https://doi.org/10.1021/acsmaterialsau.1c00041
ACS Mater. Au 2022, 2, 1−20

carbon matrix as the support which provides enormous active sites for single-metal atom anchoring.[160] Through functionalizing graphene quantum dots (GQDs) with amine groups ($GQD\text{-}NH_2$), GQDs can uniformly and stably anchor TM cations on their surfaces. The strong interaction between TM SACs and the GQDs based support and the large spacing between TM SACs leads to robust catalysts with no aggregation. In addition, Ni−N−C with a high atomic percentage (15 wt %) delivered a CO partial current of 122 mA/cm^2, representing a 2.5-fold improvement from 7.5 wt % Ni−N−C.

Also, Su et al. constructed a thermodynamics view of SAC kinetic stability (E_a) in light of the correlation between the binding energy (E_{bind}) of SACs on a support to kinetic transport features through considering the activation barrier for metal atom diffusion.[161] From the strong correlation of E_a and $(E_{bind})^2/E_c$ based on computational data, the universal correlations between E_a with the cohesive energy (E_c) of the bulk metal and E_{bind} of metal atoms to the support were derived, which can produce a precise description of SACs and this physical descriptor allows large availability in further screening.

Furthermore, because of the availability of computer hardware and computational chemistry, machine learning (ML) has recently offered special shortcuts in the rational design and development of catalysts, including advanced SACs.[162] For example, Kim et al. recently predicted efficient electrocatalysts for the electrochemical NRR using a deep neural network.[163] From the high-throughput DFT calculations on boron-doped graphene SACs, the adsorption energy and free energy were predicted via a feature-based light gradient boosting machine model. ML-assisted catalyst design enabled the validation of the catalytic activity over numerous candidates, and single-atom Cr coordinated with three boron atoms and one carbon atom embedded in the carbon supports (CrB_3C_1) was selected to be a promising electrocatalyst with a minimal overpotential of 0.13 V for NRR. In addition, Xu et al. developed a universal principle to evaluate the catalytic activity of SACs supported on a graphene for HER, OER, and ORR by proposing the descriptor that correlates with the adsorption energy of the intermediates.[164] Linear regression showed that the coordination number and the electronegativity of the metal single atom and the electronegativity of the nearest neighbor atoms were strongly responsible for the overall catalytic activity. Therefore, designing and developing multicomponent SACs might benefit from ML assistance, since the number of candidates and the complexity of the active sites increase sharply.

We believe that careful tailoring of multicomponent active sites is one of the most promising approaches to unleash the full potential of SACs and reach their superior catalytic activity, selectivity, and stability at the same time, which makes SACs promising candidates for electrocatalysts in various energy conversion reactions. The development of novel synthesis strategies for the precise control of the atomic surrounding and active centers accompanied by increasing the density of active sites in SACs should be emphasized. Also, different types of support or host materials beyond the traditional nitrogen-doped carbon materials should be explored to increase the combinational space of the multicomponent SACs and also the chances to discover optimized catalysts. The collaboration between in situ/operando characterization techniques and the advanced computational approaches might accelerate both the fundamental understanding of the multicomponent SACs and the rational development of the superior catalysts. We hope this Review paves the way for the research direction toward multicomponent SACs to rationally maximize and optimize the catalytic performance of a wide range of electrochemical reactions and offer valuable clues for ultimate solutions to the global energy crisis.

AUTHOR INFORMATION

Corresponding Authors

Soo Young Kim − *Department of Materials Science and Engineering, Korea University, Seoul 02841, Republic of Korea;* orcid.org/0000-0002-0685-7991; Email: sooyoung.kim@korea.ac.kr

Ho Won Jang − *Department of Materials Science and Engineering, Research Institute of Advanced Materials, Seoul National University, Seoul 08826, Republic of Korea; Advanced Institute of Convergence Technology, Seoul National University, Suwon 16229, Republic of Korea;* orcid.org/0000-0002-6952-7359; Email: hwjang@snu.ac.kr

Authors

Jaehyun Kim − *Department of Materials Science and Engineering, Research Institute of Advanced Materials, Seoul National University, Seoul 08826, Republic of Korea;* orcid.org/0000-0001-7039-9342

Sungkyun Choi − *Department of Materials Science and Engineering, Research Institute of Advanced Materials, Seoul National University, Seoul 08826, Republic of Korea*

Jinhyuk Cho − *Department of Materials Science and Engineering, Korea University, Seoul 02841, Republic of Korea*

Complete contact information is available at: https://pubs.acs.org/10.1021/acsmaterialsau.1c00041

Author Contributions

‖J.K., S.C., and J.C. contributed equally to this paper.

Notes

The authors declare no competing financial interest.

ACKNOWLEDGMENTS

This work was supported by the Basic Science Research Program through the National Research Foundation of Korea (NRF) funded by the Korean Ministry of Science, ICT and Future Planning (2021R1A2B5B03001851), and the Basic Research Laboratory Program through an NRF grant funded by the Korean Ministry of Science, ICT and Future Planning (2021R1A4A302787811). The Inter-University Semiconductor Research Center and Engineering Research at Seoul National University provided research facilities for this work.

REFERENCES

(1) Panwar, N. L.; Kaushik, S. C.; Kothari, S. Role of Renewable Energy Sources in Environmental Protection: A Review. *Renewable Sustainable Energy Rev.* **2011**, *15* (3), 1513−1524.

(2) Zhu, Y. P.; Guo, C.; Zheng, Y.; Qiao, S. Z. Surface and Interface Engineering of Noble-Metal-Free Electrocatalysts for Efficient Energy Conversion Processes. *Acc. Chem. Res.* **2017**, *50* (4), 915−923.

(3) Su, J.; Ge, R.; Dong, Y.; Hao, F.; Chen, L. Recent Progress in Single-Atom Electrocatalysts: Concept, Synthesis, and Applications in

Clean Energy Conversion. *J. Mater. Chem. A* **2018**, *6* (29), 14025−14042.
(4) Sun, T.; Xu, L.; Wang, D.; Li, Y. Metal Organic Frameworks Derived Single Atom Catalysts for Electrocatalytic Energy Conversion. *Nano Res.* **2019**, *12* (9), 2067−2080.
(5) Zhu, Y.; Sokolowski, J.; Song, X.; He, Y.; Mei, Y.; Wu, G. Engineering Local Coordination Environments of Atomically Dispersed and Heteroatom-Coordinated Single Metal Site Electrocatalysts for Clean Energy-Conversion. *Adv. Energy Mater.* **2020**, *10*, 1902844.
(6) Zhang, S.; Fan, Q.; Xia, R.; Meyer, T. J. CO2 Reduction: From Homogeneous to Heterogeneous Electrocatalysis. *Acc. Chem. Res.* **2020**, *53*, 255−264.
(7) Huang, Z. F.; Wang, J.; Peng, Y.; Jung, C. Y.; Fisher, A.; Wang, X. Design of Efficient Bifunctional Oxygen Reduction/Evolution Electrocatalyst: Recent Advances and Perspectives. *Adv. Energy Mater.* **2017**, *7*, 1700544.
(8) Zhu, B.; Liang, Z.; Zou, R. Designing Advanced Catalysts for Energy Conversion Based on Urea Oxidation Reaction. *Small* **2020**, *16*, 1906133.
(9) Zhao, R.; Li, Q.; Chen, Z.; Jose, V.; Jiang, X.; Fu, G.; Lee, J. M.; Huang, S. B, N-Doped Ultrathin Carbon Nanosheet Superstructure for High-Performance Oxygen Reduction Reaction in Rechargeable Zinc-Air Battery. *Carbon* **2020**, *164*, 398−406.
(10) Zhang, H.; Cheng, W.; Luan, D.; Lou, X. W. Atomically Dispersed Reactive Centers for Electrocatalytic CO2 Reduction and Water Splitting. *Angew. Chem., Int. Ed.* **2021**, *60* (24), 13177−13196.
(11) Liu, Y.; Chen, F.; Ye, W.; Zeng, M.; Han, N.; Zhao, F.; Wang, X.; Li, Y. High-Performance Oxygen Reduction Electrocatalyst Derived from Polydopamine and Cobalt Supported on Carbon Nanotubes for Metal-Air Batteries. *Adv. Funct. Mater.* **2017**, *27*, 1606034.
(12) Cui, X.; Li, W.; Ryabchuk, P.; Junge, K.; Beller, M. Bridging Homogeneous and Heterogeneous Catalysis by Heterogeneous Single-Metal-Site Catalysts. *Nat. Catal.* **2018**, *1* (6), 385−397.
(13) Astruc, D.; Lu, F.; Aranzaes, J. R. Nanoparticles as Recyclable Catalysts: The Frontier between Homogeneous and Heterogeneous Catalysis. *Angew. Chem., Int. Ed.* **2005**, *44* (48), 7852−7872.
(14) Fei, H.; Dong, J.; Chen, D.; Hu, T.; Duan, X.; Shakir, I.; Huang, Y.; Duan, X. Single Atom Electrocatalysts Supported on Graphene or Graphene-like Carbons. *Chem. Soc. Rev.* **2019**, *48* (20), 5207−5241.
(15) Wang, Y.; Mao, J.; Meng, X.; Yu, L.; Deng, D.; Bao, X. Catalysis with Two-Dimensional Materials Confining Single Atoms: Concept, Design, and Applications. *Chem. Rev.* **2019**, *119*, 1806−1854.
(16) Mitchell, S.; Vorobyeva, E.; Pérez-Ramírez, J. The Multifaceted Reactivity of Single-Atom Heterogeneous Catalysts. *Angew. Chem., Int. Ed.* **2018**, *57* (47), 15316−15329.
(17) Seh, Z. W.; Kibsgaard, J.; Dickens, C. F.; Chorkendorff, I.; Nørskov, J. K.; Jaramillo, T. F. Combining Theory and Experiment in Electrocatalysis: Insights into Materials Design. *Science (Washington, DC, U. S.)* **2017**, *355*, 146.
(18) Liu, F.; Yang, T.; Yang, J.; Xu, E.; Bajaj, A.; Kulik, H. J. Bridging the Homogeneous-Heterogeneous Divide: Modeling Spin for Reactivity in Single Atom Catalysis. *Front. Chem.* **2019**, *7*, 219.
(19) DeRita, L.; Resasco, J.; Dai, S.; Boubnov, A.; Thang, H. V.; Hoffman, A. S.; Ro, I.; Graham, G. W.; Bare, S. R.; Pacchioni, G.; Pan, X.; Christopher, P. Structural Evolution of Atomically Dispersed Pt Catalysts Dictates Reactivity. *Nat. Mater.* **2019**, *18* (7), 746−751.
(20) Xiao, M.; Zhu, J.; Li, G.; Li, N.; Li, S.; Cano, Z. P.; Ma, L.; Cui, P.; Xu, P.; Jiang, G.; Jin, H.; Wang, S.; Wu, T.; Lu, J.; Yu, A.; Su, D.; Chen, Z. A Single-Atom Iridium Heterogeneous Catalyst in Oxygen Reduction Reaction. *Angew. Chem., Int. Ed.* **2019**, *58* (28), 9640−9645.
(21) Li, X.; Yang, X.; Huang, Y.; Zhang, T.; Liu, B. Supported Noble-Metal Single Atoms for Heterogeneous Catalysis. *Adv. Mater.* **2019**, *31*, 1902031.
(22) Shi, Q.; Hwang, S.; Yang, H.; Ismail, F.; Su, D.; Higgins, D.; Wu, G. Supported and Coordinated Single Metal Site Electrocatalysts. *Mater. Today* **2020**, *37*, 93−111.
(23) Gu, J.; Hsu, C. S.; Bai, L.; Chen, H. M.; Hu, X. Atomically Dispersed Fe3+ Sites Catalyze Efficient CO2 Electroreduction to CO. *Science (Washington, DC, U. S.)* **2019**, *364* (6445), 1091−1094.
(24) Chen, Z. W.; Chen, L. X.; Yang, C. C.; Jiang, Q. Atomic (Single, Double, and Triple Atoms) Catalysis: Frontiers, Opportunities, and Challenges. *J. Mater. Chem. A* **2019**, *7* (8), 3492−3515.
(25) Han, X.; Ling, X.; Yu, D.; Xie, D.; Li, L.; Peng, S.; Zhong, C.; Zhao, N.; Deng, Y.; Hu, W. Atomically Dispersed Binary Co-Ni Sites in Nitrogen-Doped Hollow Carbon Nanocubes for Reversible Oxygen Reduction and Evolution. *Adv. Mater.* **2019**, *31*, 1905622.
(26) Lin, L.; Li, H.; Yan, C.; Li, H.; Si, R.; Li, M.; Xiao, J.; Wang, G.; Bao, X. Synergistic Catalysis over Iron-Nitrogen Sites Anchored with Cobalt Phthalocyanine for Efficient CO2 Electroreduction. *Adv. Mater.* **2019**, *31*, 1903470.
(27) Chen, J.; Li, H.; Fan, C.; Meng, Q.; Tang, Y.; Qiu, X.; Fu, G.; Ma, T. Dual Single-Atomic Ni-N4 and Fe-N4 Sites Constructing Janus Hollow Graphene for Selective Oxygen Electrocatalysis. *Adv. Mater.* **2020**, *32*, 2003134.
(28) Wang, C.; Wang, K.; Feng, Y.; Li, C.; Zhou, X.; Gan, L.; Feng, Y.; Zhou, H.; Zhang, B.; Qu, X.; Li, H.; Li, J.; Li, A.; Sun, Y.; Zhang, S.; Yang, G.; Guo, Y.; Yang, S.; Zhou, T.; Dong, F.; Zheng, K.; Wang, L.; Huang, J.; Zhang, Z.; Han, X. Co and Pt Dual-Single-Atoms with Oxygen-Coordinated Co-O-Pt Dimer Sites for Ultrahigh Photocatalytic Hydrogen Evolution Efficiency. *Adv. Mater.* **2021**, *33*, 2003327.
(29) Tong, M.; Sun, F.; Xie, Y.; Wang, Y.; Yang, Y.; Tian, C.; Wang, L.; Fu, H. Operando Cooperated Catalytic Mechanism of Atomically Dispersed Cu-N4 and Zn-N4 for Promoting Oxygen Reduction Reaction. *Angew. Chem., Int. Ed.* **2021**, *60* (25), 14005−14012.
(30) Bai, L.; Hsu, C. S.; Alexander, D. T. L.; Chen, H. M.; Hu, X. A Cobalt-Iron Double-Atom Catalyst for the Oxygen Evolution Reaction. *J. Am. Chem. Soc.* **2019**, *141* (36), 14190−14199.
(31) Xiao, M.; Zhang, H.; Chen, Y.; Zhu, J.; Gao, L.; Jin, Z.; Ge, J.; Jiang, Z.; Chen, S.; Liu, C.; Xing, W. Identification of Binuclear Co2N5 Active Sites for Oxygen Reduction Reaction with More than One Magnitude Higher Activity than Single Atom CoN4 Site. *Nano Energy* **2018**, *46*, 396−403.
(32) Liu, D.; Wang, B.; Li, H.; Huang, S.; Liu, M.; Wang, J.; Wang, Q.; Zhang, J.; Zhao, Y. Distinguished Zn,Co-Nx-C-Sy Active Sites Confined in Dentric Carbon for Highly Efficient Oxygen Reduction Reaction and Flexible Zn-Air Batteries. *Nano Energy* **2019**, *58*, 277−283.
(33) Ren, W.; Tan, X.; Yang, W.; Jia, C.; Xu, S.; Wang, K.; Smith, S. C.; Zhao, C. Isolated Diatomic Ni-Fe Metal-Nitrogen Sites for Synergistic Electroreduction of CO2. *Angew. Chem., Int. Ed.* **2019**, *58* (21), 6972−6976.
(34) Zhu, W.; Zhang, L.; Liu, S.; Li, A.; Yuan, X.; Hu, C.; Zhang, G.; Deng, W.; Zang, K.; Luo, J.; Zhu, Y.; Gu, M.; Zhao, Z. J.; Gong, J. Enhanced CO2 Electroreduction on Neighboring Zn/Co Monomers by Electronic Effect. *Angew. Chem., Int. Ed.* **2020**, *59* (31), 12664−12668.
(35) Yang, G.; Zhu, J.; Yuan, P.; Hu, Y.; Qu, G.; Lu, B. A.; Xue, X.; Yin, H.; Cheng, W.; Cheng, J.; Xu, W.; Li, J.; Hu, J.; Mu, S.; Zhang, J. N. Regulating Fe-Spin State by Atomically Dispersed Mn-N in Fe-N-C Catalysts with High Oxygen Reduction Activity. *Nat. Commun.* **2021**, *12*, 1734.
(36) Yang, Y.; Qian, Y.; Li, H.; Zhang, Z.; Mu, Y.; Do, D.; Zhou, B.; Dong, J.; Yan, W.; Qin, Y.; Fang, L.; Feng, R.; Zhou, J.; Zhang, P.; Dong, J.; Yu, G.; Liu, Y.; Zhang, X.; Fan, X. O-Coordinated W-Mo Dual-Atom Catalyst for PH-Universal Electrocatalytic Hydrogen Evolution. *Sci. Adv.* **2020**, *6*, No. eaba6586.
(37) Zhang, L.; Si, R.; Liu, H.; Chen, N.; Wang, Q.; Adair, K.; Wang, Z.; Chen, J.; Song, Z.; Li, J.; Banis, M. N.; Li, R.; Sham, T. K.; Gu, M.; Liu, L. M.; Botton, G. A.; Sun, X. Atomic Layer Deposited Pt-Ru Dual-Metal Dimers and Identifying Their Active Sites for Hydrogen Evolution Reaction. *Nat. Commun.* **2019**, *10*, 4936.
(38) Zeng, Z.; Gan, L. Y.; Bin Yang, H.; Su, X.; Gao, J.; Liu, W.; Matsumoto, H.; Gong, J.; Zhang, J.; Cai, W.; Zhang, Z.; Yan, Y.; Liu, B.; Chen, P. Orbital Coupling of Hetero-Diatomic Nickel-Iron Site for

Bifunctional Electrocatalysis of CO2 Reduction and Oxygen Evolution. *Nat. Commun.* **2021**, *12*, 4088.
(39) Zhang, N.; Zhou, T.; Ge, J.; Lin, Y.; Du, Z.; Zhong, C.; Wang, W.; et al. High-Density Planar-like Fe 2 N 6 Structure Catalyzes Efficient Oxygen Reduction High-Density Planar-like Fe 2 N 6 Structure Catalyzes Efficient Oxygen Reduction. *Matter* **2020**, *3*, 509−521.
(40) Wang, J.; Huang, Z.; Liu, W.; Chang, C.; Tang, H.; Li, Z.; Chen, W.; Jia, C.; Yao, T.; Wei, S.; Wu, Y.; Li, Y. Design of N-Coordinated Dual-Metal Sites: A Stable and Active Pt-Free Catalyst for Acidic Oxygen Reduction Reaction. *J. Am. Chem. Soc.* **2017**, *139* (48), 17281−17284.
(41) Li, Z.; He, H.; Cao, H.; Sun, S.; Diao, W.; Gao, D.; Lu, P.; Zhang, S.; Guo, Z.; Li, M.; Liu, R.; Ren, D.; Liu, C.; Zhang, Y.; Yang, Z.; Jiang, J.; Zhang, G. Atomic Co/Ni Dual Sites and Co/Ni Alloy Nanoparticles in N-Doped Porous Janus-like Carbon Frameworks for Bifunctional Oxygen Electrocatalysis. *Appl. Catal., B* **2019**, *240*, 112−121.
(42) Zhou, Y.; Yang, W.; Utetiwabo, W.; Lian, Y. M.; Yin, X.; Zhou, L.; Yu, P.; Chen, R.; Sun, S. Revealing of Active Sites and Catalytic Mechanism in N-Coordinated Fe, Ni Dual-Doped Carbon with Superior Acidic Oxygen Reduction than Single-Atom Catalyst. *J. Phys. Chem. Lett.* **2020**, *11* (4), 1404−1410.
(43) Wang, F.; Zhou, Y.; Lin, S.; Yang, L.; Hu, Z.; Xie, D. Axial Ligand Effect on the Stability of Fe-N-C Electrocatalysts for Acidic Oxygen Reduction Reaction. *Nano Energy* **2020**, *78*, 105128.
(44) Li, X.; Liu, L.; Ren, X.; Gao, J.; Huang, Y.; Liu, B. Microenvironment Modulation of Single-Atom Catalysts and Their Roles in Electrochemical Energy Conversion. *Sci. Adv.* **2020**, *6*, No. eabb6833.
(45) Lu, B.; Liu, Q.; Chen, S. Electrocatalysis of Single-Atom Sites: Impacts of Atomic Coordination. *ACS Catal.* **2020**, *10* (14), 7584−7618.
(46) Ji, S.; Chen, Y.; Wang, X.; Zhang, Z.; Wang, D.; Li, Y. Chemical Synthesis of Single Atomic Site Catalysts. *Chem. Rev.* **2020**, *120* (21), 11900−11955.
(47) Fan, M.; Cui, J.; Wu, J.; Vajtai, R.; Sun, D.; Ajayan, P. M. Improving the Catalytic Activity of Carbon-Supported Single Atom Catalysts by Polynary Metal or Heteroatom Doping. *Small* **2020**, *16*, 1906782.
(48) Li, M.; Wang, H.; Luo, W.; Sherrell, P. C.; Chen, J.; Yang, J. Heterogeneous Single-Atom Catalysts for Electrochemical CO2 Reduction Reaction. *Adv. Mater.* **2020**, *32*, 2001848.
(49) Peng, Y.; Lu, B.; Chen, S. Carbon-Supported Single Atom Catalysts for Electrochemical Energy Conversion and Storage. *Adv. Mater.* **2018**, *30*, 1801995.
(50) Gawande, M. B.; Fornasiero, P.; Zbořil, R. Carbon-Based Single-Atom Catalysts for Advanced Applications. *ACS Catal.* **2020**, *10* (3), 2231−2259.
(51) Wang, Y.; Cui, X.; Peng, L.; Li, L.; Qiao, J.; Huang, H.; Shi, J. Metal-Nitrogen-Carbon Catalysts of Specifically Coordinated Configurations toward Typical Electrochemical Redox Reactions. *Adv. Mater.* **2021**, *33*, 2100997.
(52) Shang, Y.; Xu, X.; Gao, B.; Wang, S.; Duan, X. Single-Atom Catalysis in Advanced Oxidation Processes for Environmental Remediation. *Chem. Soc. Rev.* **2021**, *50* (8), 5281−5322.
(53) Gao, J.; Tao, H.; Liu, B. Progress of Nonprecious-Metal-Based Electrocatalysts for Oxygen Evolution in Acidic Media. *Adv. Mater.* **2021**, *33*, 2003786.
(54) Zhuo, H. Y.; Zhang, X.; Liang, J. X.; Yu, Q.; Xiao, H.; Li, J. Theoretical Understandings of Graphene-Based Metal Single-Atom Catalysts: Stability and Catalytic Performance. *Chem. Rev.* **2020**, *120* (21), 12315−12341.
(55) Li, X.; Rong, H.; Zhang, J.; Wang, D.; Li, Y. Modulating the Local Coordination Environment of Single-Atom Catalysts for Enhanced Catalytic Performance. *Nano Res.* **2020**, *13* (7), 1842−1855.
(56) Zhao, C. X.; Li, B. Q.; Liu, J. N.; Zhang, Q. Intrinsic Electrocatalytic Activity Regulation of M-N-C Single-Atom Catalysts for the Oxygen Reduction Reaction. *Angew. Chem., Int. Ed.* **2021**, *60* (9), 4448−4463.
(57) Wang, J.; Li, Z.; Wu, Y.; Li, Y. Fabrication of Single-Atom Catalysts with Precise Structure and High Metal Loading. *Adv. Mater.* **2018**, *30*, 1801649.
(58) Zhou, K. L.; Wang, Z.; Han, C. B.; Ke, X.; Wang, C.; Zhang, Q.; Liu, J.; Wang, H.; Yan, H.; Jin, Y. Platinum Single-Atom Catalyst Coupled with Transition Metal/Metal Oxide Heterostructure for Accelerating Alkaline Hydrogen Evolution Reaction. *Nat. Commun.* **2021**, *12*, 3783.
(59) Lu, B.; Guo, L.; Wu, F.; Peng, Y.; Lu, J. E.; Smart, T. J.; Wang, N.; Finfrock, Y. Z.; Morris, D.; Zhang, P.; Li, N.; Gao, P.; Ping, Y.; Chen, S. Ruthenium Atomically Dispersed in Carbon Outperforms Platinum toward Hydrogen Evolution in Alkaline Media. *Nat. Commun.* **2019**, *10*, 631.
(60) Fei, H.; Dong, J.; Arellano-Jimenez, M. J.; Ye, G.; Kim, N. D.; Samuel, E. L. G.; Peng, Z.; Zhu, Z.; Qin, F.; Bao, J.; Yacaman, M. J.; Ajayan, P. M.; Chen, D.; Tour, J. M. Atomic Cobalt on Nitrogen-Doped Graphene for Hydrogen Generation. *Nat. Commun.* **2015**, *6*, 8668.
(61) Cao, L.; Luo, Q.; Liu, W.; Lin, Y.; Liu, X.; Cao, Y.; Zhang, W.; Wu, Y.; Yang, J.; Yao, T.; Wei, S. Identification of Single-Atom Active Sites in Carbon-Based Cobalt Catalysts during Electrocatalytic Hydrogen Evolution. *Nat. Catal.* **2019**, *2* (2), 134−141.
(62) Yang, J.; Li, W. H.; Tan, S.; Xu, K.; Wang, Y.; Wang, D.; Li, Y. The Electronic Metal-Support Interaction Directing the Design of Single Atomic Site Catalysts: Achieving High Efficiency Towards Hydrogen Evolution. *Angew. Chem., Int. Ed.* **2021**, *60* (35), 19085−19091.
(63) Zhao, Y.; Ling, T.; Chen, S.; Jin, B.; Vasileff, A.; Jiao, Y.; Song, L.; Luo, J.; Qiao, S. Z. Non-Metal Single-Iodine-Atom Electrocatalysts for the Hydrogen Evolution Reaction. *Angew. Chem., Int. Ed.* **2019**, *58* (35), 12252−12257.
(64) Fei, H.; Dong, J.; Feng, Y.; Allen, C. S.; Wan, C.; Volosskiy, B.; Li, M.; Zhao, Z.; Wang, Y.; Sun, H.; An, P.; Chen, W.; Guo, Z.; Lee, C.; Chen, D.; Shakir, I.; Liu, M.; Hu, T.; Li, Y.; Kirkland, A. I.; Duan, X.; Huang, Y. General Synthesis and Definitive Structural Identification of MN4C4 Single-Atom Catalysts with Tunable Electrocatalytic Activities. *Nat. Catal.* **2018**, *1* (1), 63−72.
(65) Cao, L.; Luo, Q.; Chen, J.; Wang, L.; Lin, Y.; Wang, H.; Liu, X.; Shen, X.; Zhang, W.; Liu, W.; Qi, Z.; Jiang, Z.; Yang, J.; Yao, T. Dynamic Oxygen Adsorption on Single-Atomic Ruthenium Catalyst with High Performance for Acidic Oxygen Evolution Reaction. *Nat. Commun.* **2019**, *10*, 4849.
(66) Shan, J.; Ye, C.; Chen, S.; Sun, T.; Jiao, Y.; Liu, L.; Zhu, C.; Song, L.; Han, Y.; Jaroniec, M.; Zhu, Y.; Zheng, Y.; Qiao, S. Z. Short-Range Ordered Iridium Single Atoms Integrated into Cobalt Oxide Spinel Structure for Highly Efficient Electrocatalytic Water Oxidation. *J. Am. Chem. Soc.* **2021**, *143* (13), 5201−5211.
(67) Li, Z.; Niu, W.; Yang, Z.; Zaman, N.; Samarakoon, W.; Wang, M.; Kara, A.; Lucero, M.; Vyas, M. V.; Cao, H.; Zhou, H.; Sterbinsky, G. E.; Feng, Z.; Du, Y.; Yang, Y. Stabilizing Atomic Pt with Trapped Interstitial F in Alloyed PtCo Nanosheets for High-Performance Zinc-Air Batteries. *Energy Environ. Sci.* **2020**, *13* (3), 884−895.
(68) Zhang, J.; Zhao, Y.; Chen, C.; Huang, Y. C.; Dong, C. L.; Chen, C. J.; Liu, R. S.; Wang, C.; Yan, K.; Li, Y.; Wang, G. Tuning the Coordination Environment in Single-Atom Catalysts to Achieve Highly Efficient Oxygen Reduction Reactions. *J. Am. Chem. Soc.* **2019**, *141* (51), 20118−20126.
(69) Wu, F.; Pan, C.; He, C. T.; Han, Y.; Ma, W.; Wei, H.; Ji, W.; Chen, W.; Mao, J.; Yu, P.; Wang, D.; Mao, L.; Li, Y. Single-Atom Co-N4 Electrocatalyst Enabling Four-Electron Oxygen Reduction with Enhanced Hydrogen Peroxide Tolerance for Selective Sensing. *J. Am. Chem. Soc.* **2020**, *142* (39), 16861−16867.
(70) Jung, E.; Shin, H.; Lee, B.; Efremov, V.; Lee, S.; Lee, H. S.; Kim, J.; Antink, W. H.; Park, S.; Lee, K.; Cho, S.; Yoo, J. S.; Sung, Y.; Hyeon, T. Atomic-Level Tuning of Co-N-C Catalyst for High-Performance Electrochemical H2O2 Production. *Nat. Mater.* **2020**, *19*, 436−422.

(71) Tang, C.; Chen, L.; Li, H.; Li, L.; Jiao, Y.; Zheng, Y.; Xu, H.; Davey, K.; Qiao, S. Z. Tailoring Acidic Oxygen Reduction Selectivity on Single-Atom Catalysts via Modification of First and Second Coordination Spheres. *J. Am. Chem. Soc.* **2021**, *143* (20), 7819−7827.
(72) Wang, X. X.; Cullen, D. A.; Pan, Y. T.; Hwang, S.; Wang, M.; Feng, Z.; Wang, J.; Engelhard, M. H.; Zhang, H.; He, Y.; Shao, Y.; Su, D.; More, K. L.; Spendelow, J. S.; Wu, G. Nitrogen-Coordinated Single Cobalt Atom Catalysts for Oxygen Reduction in Proton Exchange Membrane Fuel Cells. *Adv. Mater.* **2018**, *30*, 1706758.
(73) Han, A.; Wang, X.; Tang, K.; Zhang, Z.; Ye, C.; Kong, K.; Hu, H.; Zheng, L.; Jiang, P.; Zhao, C.; Zhang, Q.; Wang, D.; Li, Y. An Adjacent Atomic Platinum Site Enables Single-Atom Iron with High Oxygen Reduction Reaction Performance. *Angew. Chem., Int. Ed.* **2021**, *60* (35), 19262−19271.
(74) Vasileff, A.; Zhu, Y.; Zhi, X.; Zhao, Y.; Ge, L.; Chen, H. M.; Zheng, Y.; Qiao, S. Z. Electrochemical Reduction of CO2 to Ethane through Stabilization of an Ethoxy Intermediate. *Angew. Chem., Int. Ed.* **2020**, *59* (44), 19649−19653.
(75) Yao, D.; Tang, C.; Vasileff, A.; Zhi, X.; Jiao, Y.; Qiao, S. Z. The Controllable Reconstruction of Bi-MOFs for Electrochemical CO2 Reduction through Electrolyte and Potential Mediation. *Angew. Chem., Int. Ed.* **2021**, *60* (33), 18178−18184.
(76) Cai, Y.; Fu, J.; Zhou, Y.; Chang, Y. C.; Min, Q.; Zhu, J. J.; Lin, Y.; Zhu, W. Insights on Forming N,O-Coordinated Cu Single-Atom Catalysts for Electrochemical Reduction CO2 to Methane. *Nat. Commun.* **2021**, *12*, 586.
(77) Ju, W.; Bagger, A.; Hao, G. P.; Varela, A. S.; Sinev, I.; Bon, V.; Roldan Cuenya, B.; Kaskel, S.; Rossmeisl, J.; Strasser, P. Understanding Activity and Selectivity of Metal-Nitrogen-Doped Carbon Catalysts for Electrochemical Reduction of CO2. *Nat. Commun.* **2017**, *8*, 944.
(78) Zhang, N.; Zhang, X.; Kang, Y.; Ye, C.; Jin, R.; Yan, H.; Lin, R.; Yang, J.; Xu, Q.; Wang, Y.; Zhang, Q.; Gu, L.; Liu, L.; Song, W.; Liu, J.; Wang, D.; Li, Y. A Supported Pd2 Dual-Atom Site Catalyst for Efficient Electrochemical CO2 Reduction. *Angew. Chem., Int. Ed.* **2021**, *60* (24), 13388−13393.
(79) Liu, X.; Jiao, Y.; Zheng, Y.; Jaroniec, M.; Qiao, S. Z. Building Up a Picture of the Electrocatalytic Nitrogen Reduction Activity of Transition Metal Single-Atom Catalysts. *J. Am. Chem. Soc.* **2019**, *141* (24), 9664−9672.
(80) Geng, Z.; Liu, Y.; Kong, X.; Li, P.; Li, K.; Liu, Z.; Du, J.; Shu, M.; Si, R.; Zeng, J. Achieving a Record-High Yield Rate of 120.9 Mg NH3Mg Cat.-1 H-1 for N2 Electrochemical Reduction over Ru Single-Atom Catalysts. *Adv. Mater.* **2018**, *30*, 1803498.
(81) Zang, W.; Yang, T.; Zou, H.; Xi, S.; Zhang, H.; Liu, X.; Kou, Z.; Du, Y.; Feng, Y. P.; Shen, L.; Duan, L.; Wang, J.; Pennycook, S. J. Copper Single Atoms Anchored in Porous Nitrogen-Doped Carbon as Efficient PH-Universal Catalysts for the Nitrogen Reduction Reaction. *ACS Catal.* **2019**, *9* (11), 10166−10173.
(82) Liu, C.; Li, Q.; Wu, C.; Zhang, J.; Jin, Y.; Macfarlane, D. R.; Sun, C. Single-Boron Catalysts for Nitrogen Reduction Reaction. *J. Am. Chem. Soc.* **2019**, *141* (7), 2884−2888.
(83) Zhao, W.; Zhang, L.; Luo, Q.; Hu, Z.; Zhang, W.; Smith, S.; Yang, J. Single Mo1(Cr1) Atom on Nitrogen-Doped Graphene Enables Highly Selective Electroreduction of Nitrogen into Ammonia. *ACS Catal.* **2019**, *9* (4), 3419−3425.
(84) Mahmood, A.; Guo, W.; Tabassum, H.; Zou, R. Metal-organic Framework-based Nanomaterials for Electrocatalysis. *Adv. Energy Mater.* **2016**, *6*, 1600423.
(85) Chen, Y.-Z.; Zhang, R.; Jiao, L.; Jiang, H.-L. Metal-Organic Framework-Derived Porous Materials for Catalysis. *Coord. Chem. Rev.* **2018**, *362*, 1−23.
(86) Khalid, M.; Honorato, A. M. B.; Varela, H.; Dai, L. Multifunctional Electrocatalysts Derived from Conducting Polymer and Metal Organic Framework Complexes. *Nano Energy* **2018**, *45*, 127−135.
(87) Li, A.; Song, H.; Bian, Z.; Shi, L.; Chen, X.; Zhou, J. ZnO Nanosheet/Squeezebox-like Porous Carbon Composites Synthesized by in Situ Pyrolysis of a Mixed-Ligand Metal-Organic Framework. *J. Mater. Chem. A* **2017**, *5* (12), 5934−5942.
(88) Xuan, W.; Zhu, C.; Liu, Y.; Cui, Y. Mesoporous Metal-Organic Framework Materials. *Chem. Soc. Rev.* **2012**, *41* (5), 1677−1695.
(89) Appelhans, L. N.; Hughes, L.; McKenzie, B.; Rodriguez, M.; Griego, J.; Briscoe, J.; Moorman, M.; Frederick, E.; Wright, J. B. Facile Microwave Synthesis of Zirconium Metal-Organic Framework Thin Films on Gold and Silicon and Application to Sensor Functionalization. *Microporous Mesoporous Mater.* **2021**, *323*, 111133.
(90) Lee, H. J.; Choi, S.; Oh, M. Well-Dispersed Hollow Porous Carbon Spheres Synthesized by Direct Pyrolysis of Core-Shell Type Metal-Organic Frameworks and Their Sorption Properties. *Chem. Commun.* **2014**, *50* (34), 4492−4495.
(91) Luo, E.; Wang, C.; Li, Y.; Wang, X.; Gong, L.; Zhao, T.; Jin, Z.; Ge, J.; Liu, C.; Xing, W. Accelerated Oxygen Reduction on Fe/N/C Catalysts Derived from Precisely-Designed ZIF Precursors. *Nano Res.* **2020**, *13* (9), 2420−2426.
(92) Li, Y.; Wu, J.; Zhang, B.; Wang, W.; Zhang, G.; Seh, Z. W.; Zhang, N.; Sun, J.; Huang, L.; Jiang, J.; et al. Fast Conversion and Controlled Deposition of Lithium (Poly) Sulfides in Lithium-Sulfur Batteries Using High-Loading Cobalt Single Atoms. *Energy Storage Mater.* **2020**, *30*, 250−259.
(93) Li, H.; Su, Y.; Sun, W.; Wang, Y. Carbon Nanotubes Rooted in Porous Ternary Metal Sulfide@ N/S-Doped Carbon Dodecahedron: Bimetal-Organic-Frameworks Derivation and Electrochemical Application for High-Capacity and Long-Life Lithium-Ion Batteries. *Adv. Funct. Mater.* **2016**, *26* (45), 8345−8353.
(94) Yan, C.; Li, H.; Ye, Y.; Wu, H.; Cai, F.; Si, R.; Xiao, J.; Miao, S.; Xie, S.; Yang, F. Coordinatively Unsaturated Nickel-Nitrogen Sites towards Selective and High-Rate CO 2 Electroreduction. *Energy Environ. Sci.* **2018**, *11* (5), 1204−1210.
(95) Fu, J.; Dong, J.; Si, R.; Sun, K.; Zhang, J.; Li, M.; Yu, N.; Zhang, B.; Humphrey, M. G.; Fu, Q.; Huang, J. Synergistic Effects for Enhanced Catalysis in a Dual Single-Atom Catalyst. *ACS Catal.* **2021**, *11* (4), 1952−1961.
(96) Zhang, L.; Fischer, J. M. T. A.; Jia, Y.; Yan, X.; Xu, W.; Wang, X.; Chen, J.; Yang, D.; Liu, H.; Zhuang, L.; Hankel, M.; Searles, D. J.; Huang, K.; Feng, S.; Brown, C. L.; Yao, X. Coordination of Atomic Co-Pt Coupling Species at Carbon Defects as Active Sites for Oxygen Reduction Reaction. *J. Am. Chem. Soc.* **2018**, *140* (34), 10757−10763.
(97) Fonseca, J.; Lu, J. Single-Atom Catalysts Designed and Prepared by the Atomic Layer Deposition Technique. *ACS Catal.* **2021**, *11*, 7018−7059.
(98) Puurunen, R. L. A Short History of Atomic Layer Deposition: Tuomo Suntola's Atomic Layer Epitaxy. *Chem. Vap. Deposition* **2014**, *20* (10−12), 332−344.
(99) Farm, E.; Kemell, M.; Ritala, M.; Leskelä, M. Selective-Area Atomic Layer Deposition Using Poly (Methyl Methacrylate) Films as Mask Layers. *J. Phys. Chem. C* **2008**, *112* (40), 15791−15795.
(100) Cheng, N.; Shao, Y.; Liu, J.; Sun, X. Electrocatalysts by Atomic Layer Deposition for Fuel Cell Applications. *Nano Energy* **2016**, *29*, 220−242.
(101) Kim, K.; Lee, H.-B.-R.; Johnson, R. W.; Tanskanen, J. T.; Liu, N.; Kim, M.-G.; Pang, C.; Ahn, C.; Bent, S. F.; Bao, Z. Selective Metal Deposition at Graphene Line Defects by Atomic Layer Deposition. *Nat. Commun.* **2014**, *5*, 4781.
(102) Wang, X.; Jin, B.; Jin, Y.; Wu, T.; Ma, L.; Liang, X. Supported Single Fe Atoms Prepared via Atomic Layer Deposition for Catalytic Reactions. *ACS Appl. Nano Mater.* **2020**, *3* (3), 2867−2874.
(103) Ge, X.; Su, G.; Che, W.; Yang, J.; Zhou, X.; Wang, Z.; Qu, Y.; Yao, T.; Liu, W.; Wu, Y. Atomic Filtration by Graphene Oxide Membranes to Access Atomically Dispersed Single Atom Catalysts. *ACS Catal.* **2020**, *10* (18), 10468−10475.
(104) Huang, X.; Xia, Y.; Cao, Y.; Zheng, X.; Pan, H.; Zhu, J.; Ma, C.; Wang, H.; Li, J.; You, R.; et al. Enhancing Both Selectivity and Coking-Resistance of a Single-Atom Pd 1/C 3 N 4 Catalyst for Acetylene Hydrogenation. *Nano Res.* **2017**, *10* (4), 1302−1312.
(105) Zhu, C.; Fu, S.; Shi, Q.; Du, D.; Lin, Y. Single-atom Electrocatalysts. *Angew. Chem., Int. Ed.* **2017**, *56* (45), 13944−13960.

(106) Fang, S.; Zhu, X.; Liu, X.; Gu, J.; Liu, W.; Wang, D.; Zhang, W.; Lin, Y.; Lu, J.; Wei, S.; et al. Uncovering Near-Free Platinum Single-Atom Dynamics during Electrochemical Hydrogen Evolution Reaction. *Nat. Commun.* **2020**, *11*, 1029.
(107) Zhang, Z.; Zhu, Y.; Asakura, H.; Zhang, B.; Zhang, J.; Zhou, M.; Han, Y.; Tanaka, T.; Wang, A.; Zhang, T.; et al. Thermally Stable Single Atom Pt/m-Al 2 O 3 for Selective Hydrogenation and CO Oxidation. *Nat. Commun.* **2017**, *8*, 16100.
(108) Lin, J.; Qiao, B.; Li, N.; Li, L.; Sun, X.; Liu, J.; Wang, X.; Zhang, T. Little Do More: A Highly Effective Pt 1/FeO x Single-Atom Catalyst for the Reduction of NO by H 2. *Chem. Commun.* **2015**, *51* (37), 7911−7914.
(109) Li, M.; Duanmu, K.; Wan, C.; Cheng, T.; Zhang, L.; Dai, S.; Chen, W.; Zhao, Z.; Li, P.; Fei, H.; et al. Single-Atom Tailoring of Platinum Nanocatalysts for High-Performance Multifunctional Electrocatalysis. *Nat. Catal.* **2019**, *2* (6), 495−503.
(110) Zhang, L.; Filot, I. A. W.; Su, Y.-Q.; Liu, J.-X.; Hensen, E. J. M. Understanding the Impact of Defects on Catalytic CO Oxidation of LaFeO3-Supported Rh, Pd, and Pt Single-Atom Catalysts. *J. Phys. Chem. C* **2019**, *123* (12), 7290−7298.
(111) Zhang, L.; Liu, H.; Liu, S.; Norouzi Banis, M.; Song, Z.; Li, J.; Yang, L.; Markiewicz, M.; Zhao, Y.; Li, R.; et al. Pt/Pd Single-Atom Alloys as Highly Active Electrochemical Catalysts and the Origin of Enhanced Activity. *ACS Catal.* **2019**, *9* (10), 9350−9358.
(112) Lotfi, N.; Shahrabi, T.; Yaghoubinezhad, Y.; Darband, G. B. Electrodeposition of Cedar Leaf-like Graphene Oxide@ Ni-Cu@ Ni Foam Electrode as a Highly Efficient and Ultra-Stable Catalyst for Hydrogen Evolution Reaction. *Electrochim. Acta* **2019**, *326*, 134949.
(113) Gurrappa, I.; Binder, L. Electrodeposition of Nanostructured Coatings and Their Characterization—a Review. *Sci. Technol. Adv. Mater.* **2008**, *9*, 043001.
(114) Ye, F.; Xu, C.; Liu, G.; Yuan, M.; Wang, Z.; Du, X.; Lee, J. K. Effect of Pulse Electrodeposition Parameters on Electrocatalytic the Activity of Methanol Oxidation and Morphology of Pt/C Catalyst for Direct Methanol Fuel Cells. *Energy Convers. Manage.* **2018**, *160*, 85−92.
(115) Peters, B. K.; Rodriguez, K. X.; Reisberg, S. H.; Beil, S. B.; Hickey, D. P.; Kawamata, Y.; Collins, M.; Starr, J.; Chen, L.; Udyavara, S. Scalable and Safe Synthetic Organic Electroreduction Inspired by Li-Ion Battery Chemistry. *Science (Washington, DC, U. S.)* **2019**, *363* (6429), 838−845.
(116) Wang, J.; Yoshida, A.; Wang, P.; Yu, T.; Wang, Z.; Hao, X.; Abudula, A.; Guan, G. Catalytic Oxidation of Volatile Organic Compound over Cerium Modified Cobalt-Based Mixed Oxide Catalysts Synthesized by Electrodeposition Method. *Appl. Catal., B* **2020**, *271*, 118941.
(117) Bose, R.; Karuppasamy, K.; Rajan, H.; Velusamy, D. B.; Kim, H.-S.; Alfantazi, A. Electrodeposition of Unary Oxide on a Bimetallic Hydroxide as a Highly Active and Stable Catalyst for Water Oxidation. *ACS Sustainable Chem. Eng.* **2019**, *7* (19), 16392−16400.
(118) Qiu, Y.-L.; Zhong, H.-X.; Zhang, T.-T.; Xu, W.-B.; Li, X.-F.; Zhang, H.-M. Copper Electrode Fabricated via Pulse Electrodeposition: Toward High Methane Selectivity and Activity for CO2 Electroreduction. *ACS Catal.* **2017**, *7* (9), 6302−6310.
(119) Walsh, F. C.; Wang, S.; Zhou, N. The Electrodeposition of Composite Coatings: Diversity, Applications and Challenges. *Curr. Opin. Electrochem.* **2020**, *20*, 8−19.
(120) Xu, J.; Li, R.; Xu, C.-Q.; Zeng, R.; Jiang, Z.; Mei, B.; Li, J.; Meng, D.; Chen, J. Underpotential-Deposition Synthesis and in-Line Electrochemical Analysis of Single-Atom Copper Electrocatalysts. *Appl. Catal., B* **2021**, *289*, 120028.
(121) Mayet, N.; Servat, K.; Kokoh, K. B.; Napporn, T. W. Probing the Surface of Noble Metals Electrochemically by Underpotential Deposition of Transition Metals. *Surfaces* **2019**, *2* (2), 257−276.
(122) Chen, C.; Wu, D.; Li, Z.; Zhang, R.; Kuai, C.; Zhao, X.; Dong, C.; Qiao, S.; Liu, H.; Du, X. Ruthenium-based Single-atom Alloy with High Electrocatalytic Activity for Hydrogen Evolution. *Adv. Energy Mater.* **2019**, *9* (20), 1803913.
(123) Shi, Y.; Huang, W.-M. M.; Li, J.; Zhou, Y.; Li, Z.-Q. Q.; Yin, Y.-C. C.; Xia, X.-H. H. Site-Specific Electrodeposition Enables Self-Terminating Growth of Atomically Dispersed Metal Catalysts. *Nat. Commun.* **2020**, *11*, 4558.
(124) Venkata Guru Raghavendra, K.; Sreekanth, T.V.M.; Kim, J.; Yoo, K. Novel Hydrothermal Synthesis of Jasmine Petal-like Nanoflower WS2/ZnCo2O4 as Efficient Electrode Material for High-Performance Supercapacitors. *Mater. Lett.* **2021**, *285*, 129133.
(125) Zhang, L.; Tong, R.; Ge, W.; Guo, R.; Shirsath, S. E.; Zhu, J. Facile One-Step Hydrothermal Synthesis of SnO2Microspheres with Oxygen Vacancies for Superior Ethanol Sensor. *J. Alloys Compd.* **2020**, *814*, 152266.
(126) Zhu, L.; Zeng, W.; Yang, J.; Li, Y. One-Step Hydrothermal Fabrication of Nanosheet-Assembled NiO/ZnO Microflower and Its Ethanol Sensing Property. *Ceram. Int.* **2018**, *44* (16), 19825−19830.
(127) Fang, M.; Dong, G.; Wei, R.; Ho, J. C. Hierarchical Nanostructures: Design for Sustainable Water Splitting. *Adv. Energy Mater.* **2017**, *7*, 1700559.
(128) Lu, F.; Wang, J.; Sun, X.; Chang, Z. 3D Hierarchical Carbon Nanofibers/TiO2@ MoS2 Core-Shell Heterostructures by Electrospinning, Hydrothermal and in-Situ Growth for Flexible Electrode Materials. *Mater. Des.* **2020**, *189*, 108503.
(129) Li, C.; Chen, S.; Wang, Y.; Hou, Z. ZnO/ZnS Heterostructures Grown on Zn Foil Substrate by Hydrothermal Method for Photoelectrochemical Water Splitting. *Int. J. Hydrogen Energy* **2019**, *44* (47), 25416−25427.
(130) Wang, J.; Fang, W.; Hu, Y.; Zhang, Y.; Dang, J.; Wu, Y.; Chen, B.; Zhao, H.; Li, Z. Single Atom Ru Doping 2H-MoS2 as Highly Efficient Hydrogen Evolution Reaction Electrocatalyst in a Wide PH Range. *Appl. Catal., B* **2021**, *298*, 120490.
(131) Li, X.; Xu, Y.; Zhang, C.; Wang, H.; Song, Y.; Zhang, W.; Li, C. H2O2-Assisted Hydrothermal Synthesis of TiO2-SiO2 and Its Enhanced Photocatalytic-Adsorptive Desulfurization Performance for Model Fuel. *Fuel* **2018**, *226*, 527−535.
(132) Zhang, Y.; Zhang, S.; Li, H.; Wang, C.; Jiang, F.; Lyu, J. Treatment of Municipal Sludge by Hydrothermal Oxidation Process with H2O2. *Chemosphere* **2020**, *257*, 127140.
(133) Ma, Y.; Fan, H.; Wu, C.; Zhang, M.; Yu, J.; Song, L.; Li, K.; He, J. An Efficient Dual-Metal Single-Atom Catalyst for Bifunctional Catalysis in Zinc-Air Batteries. *Carbon* **2021**, *185*, 526−535.
(134) Yang, S.; Tak, Y. J.; Kim, J.; Soon, A.; Lee, H. Support Effects in Single-Atom Platinum Catalysts for Electrochemical Oxygen Reduction. *ACS Catal.* **2017**, *7* (2), 1301−1307.
(135) Liu, Q.; Zhang, Z. Platinum Single-Atom Catalysts: A Comparative Review towards Effective Characterization. *Catal. Sci. Technol.* **2019**, *9* (18), 4821−4834.
(136) Yan, H.; Cheng, H.; Yi, H.; Lin, Y.; Yao, T.; Wang, C.; Li, J.; Wei, S.; Lu, J. Single-Atom Pd1/Graphene Catalyst Achieved by Atomic Layer Deposition: Remarkable Performance in Selective Hydrogenation of 1, 3-Butadiene. *J. Am. Chem. Soc.* **2015**, *137* (33), 10484−10487.
(137) Rajabalinia, N.; Hamzehlou, S.; Modin, E.; Chuvilin, A.; Leiza, J. R.; Asua, J. M. Coupling HAADF-STEM Tomography and Image Reconstruction for the Precise Characterization of Particle Morphology of Composite Polymer Latexes. *Macromolecules* **2019**, *52* (14), 5298−5306.
(138) Duan, S.; Wang, R.; Liu, J. Stability Investigation of a High Number Density Pt1/Fe2O3 Single-Atom Catalyst under Different Gas Environments by HAADF-STEM. *Nanotechnology* **2018**, *29*, 204002.
(139) Kirkland, A. I.; Haigh, S.; Chang, L. Y. Aberration Corrected TEM: Current Status and Future Prospects. *J. Phys. Conf. Ser.* **2008**, *126*, 012034.
(140) Hetherington, C. Aberration Correction for TEM. *Mater. Today* **2004**, *7* (12), 50−55.
(141) Li, X.; Yang, X.; Zhang, J.; Huang, Y.; Liu, B. In Situ/Operando Techniques for Characterization of Single-Atom Catalysts. *ACS Catal.* **2019**, *9* (3), 2521−2531.

(142) Gai, P. L.; Lari, L.; Ward, M. R.; Boyes, E. D. Visualisation of Single Atom Dynamics and Their Role in Nanocatalysts under Controlled Reaction Environments. *Chem. Phys. Lett.* **2014**, *592*, 355−359.
(143) Xi, W.; Wang, K.; Shen, Y.; Ge, M.; Deng, Z.; Zhao, Y.; Cao, Q.; Ding, Y.; Hu, G.; Luo, J. Dynamic Co-Catalysis of Au Single Atoms and Nanoporous Au for Methane Pyrolysis. *Nat. Commun.* **2020**, *11*, 1919.
(144) Qi, K.; Cui, X.; Gu, L.; Yu, S.; Fan, X.; Luo, M.; Xu, S.; Li, N.; Zheng, L.; Zhang, Q.; Ma, J.; Gong, Y.; Lv, F.; Wang, K.; Huang, H.; Zhang, W.; Guo, S.; Zheng, W.; Liu, P. Single-Atom Cobalt Array Bound to Distorted 1T MoS2 with Ensemble Effect for Hydrogen Evolution Catalysis. *Nat. Commun.* **2019**, *10*, 5231.
(145) Liu, K.; Zhao, X.; Ren, G.; Yang, T.; Ren, Y.; Lee, A. F.; Su, Y.; Pan, X.; Zhang, J.; Chen, Z.; Yang, J.; Liu, X.; Zhou, T.; Xi, W.; Luo, J.; Zeng, C.; Matsumoto, H.; Liu, W.; Jiang, Q.; Wilson, K.; Wang, A.; Qiao, B.; Li, W.; Zhang, T. Strong Metal-Support Interaction Promoted Scalable Production of Thermally Stable Single-Atom Catalysts. *Nat. Commun.* **2020**, *11*, 1263.
(146) Wang, A.; Li, J.; Zhang, T. Heterogeneous Single-Atom Catalysis. *Nat. Rev. Chem.* **2018**, *2* (6), 65−81.
(147) Gong, S.; Wang, C.; Jiang, P.; Hu, L.; Lei, H.; Chen, Q. Designing Highly Efficient Dual-Metal Single-Atom Electrocatalysts for the Oxygen Reduction Reaction Inspired by Biological Enzyme Systems. *J. Mater. Chem. A* **2018**, *6* (27), 13254−13262.
(148) Xiao, M.; Zhu, J.; Ma, L.; Jin, Z.; Ge, J.; Deng, X.; Hou, Y.; He, Q.; Li, J.; Jia, Q.; Mukerjee, S.; Yang, R.; Jiang, Z.; Su, D.; Liu, C.; Xing, W. Microporous Framework Induced Synthesis of Single-Atom Dispersed Fe-N-C Acidic ORR Catalyst and Its in Situ Reduced Fe-N4 Active Site Identification Revealed by X-Ray Absorption Spectroscopy. *ACS Catal.* **2018**, *8* (4), 2824−2832.
(149) Hannagan, R. T.; Patel, D. A.; Cramer, L. A.; Schilling, A. C.; Ryan, P. T. P.; Larson, A. M.; Çınar, V.; Wang, Y.; Balema, T. A.; Sykes, E. C. H. Combining STM, RAIRS and TPD to Decipher the Dispersion and Interactions Between Active Sites in RhCu Single-Atom Alloys. *ChemCatChem* **2020**, *12* (2), 488−493.
(150) Feng, J.; Gao, H.; Zheng, L.; Chen, Z.; Zeng, S.; Jiang, C.; Dong, H.; Liu, L.; Zhang, S.; Zhang, X. A Mn-N3 Single-Atom Catalyst Embedded in Graphitic Carbon Nitride for Efficient CO2 Electroreduction. *Nat. Commun.* **2020**, *11*, 4341.
(151) Yu, D.; Ma, Y.; Hu, F.; Lin, C. C.; Li, L.; Chen, H. Y.; Han, X.; Peng, S. Dual-Sites Coordination Engineering of Single Atom Catalysts for Flexible Metal-Air Batteries. *Adv. Energy Mater.* **2021**, *11*, 2101242.
(152) Ren, C.; Jiang, Q.; Lin, W.; Zhang, Y.; Huang, S.; Ding, K.; Ding, K. Density Functional Theory Study of Single-Atom V, Nb, and Ta Catalysts on Graphene and Carbon Nitride for Selective Nitrogen Reduction. *ACS Appl. Nano Mater.* **2020**, *3* (6), 5149−5159.
(153) Qin, Y. Y.; Su, Y. Q. A DFT Study on Heterogeneous Pt/CeO2(110) Single Atom Catalysts for CO Oxidation. *ChemCatChem* **2021**, *13*, 3857.
(154) Cheng, N.; Zhang, L.; Doyle-Davis, K.; Sun, X. *Single-Atom Catalysts: From Design to Application*; Springer: Singapore, 2019; Vol. 2.
(155) Man, I. C.; Su, H. Y.; Calle-Vallejo, F.; Hansen, H. A.; Martínez, J. I.; Inoglu, N. G.; Kitchin, J.; Jaramillo, T. F.; Nørskov, J. K.; Rossmeisl, J. Universality in Oxygen Evolution Electrocatalysis on Oxide Surfaces. *ChemCatChem* **2011**, *3* (7), 1159−1165.
(156) Gong, L.; Zhang, D.; Lin, C. Y.; Zhu, Y.; Shen, Y.; Zhang, J.; Han, X.; Zhang, L.; Xia, Z. Catalytic Mechanisms and Design Principles for Single-Atom Catalysts in Highly Efficient CO2 Conversion. *Adv. Energy Mater.* **2019**, *9*, 1902625.
(157) Li, L.; Chang, X.; Lin, X.; Zhao, Z. J.; Gong, J. Theoretical Insights into Single-Atom Catalysts. *Chem. Soc. Rev.* **2020**, *49* (22), 8156−8178.
(158) Niu, W. J.; He, J. Z.; Gu, B. N.; Liu, M. C.; Chueh, Y. L. Opportunities and Challenges in Precise Synthesis of Transition Metal Single-Atom Supported by 2D Materials as Catalysts toward Oxygen Reduction Reaction. *Adv. Funct. Mater.* **2021**, *31*, 2103558.
(159) Feng, K.; Zhang, H.; Gao, J.; Xu, J.; Dong, Y.; Kang, Z.; Zhong, J. Single Atoms or Not? The Limitation of EXAFS. *Appl. Phys. Lett.* **2020**, *116* (19), 191903.
(160) Xia, C.; Qiu, Y.; Xia, Y.; Zhu, P.; King, G.; Zhang, X.; Wu, Z.; Kim, J. Y.; Cullen, D. A.; Zheng, D.; Li, P.; Shakouri, M.; Heredia, E.; Cui, P.; Alshareef, H. N.; Hu, Y.; Wang, H. General Synthesis of Single-Atom Catalysts with High Metal Loading Using Graphene Quantum Dots. *Nat. Chem.* **2021**, *13*, 887−894.
(161) Su, Y. Q.; Zhang, L.; Wang, Y.; Liu, J. X.; Muravev, V.; Alexopoulos, K.; Filot, I. A. W.; Vlachos, D. G.; Hensen, E. J. M. Stability of Heterogeneous Single-Atom Catalysts: A Scaling Law Mapping Thermodynamics to Kinetics. *npj Comput. Mater.* **2020**, *6*, 144.
(162) Kim, J.; Kang, D.; Kim, S.; Jang, H. W. Catalyze Materials Science with Machine Learning. *ACS Mater. Lett.* **2021**, *3* (8), 1151−1171.
(163) Zafari, M.; Kumar, D.; Umer, M.; Kim, K. S. Machine Learning-Based High Throughput Screening for Nitrogen Fixation on Boron-Doped Single Atom Catalysts. *J. Mater. Chem. A* **2020**, *8* (10), 5209−5216.
(164) Xu, H.; Cheng, D.; Cao, D.; Zeng, X. C. A Universal Principle for a Rational Design of Single-Atom Electrocatalysts. *Nat. Catal.* **2018**, *1* (5), 339−348.

https://doi.org/10.1021/acsmaterialsau.1c00041
ACS Mater. Au 2022, 2, 1−20